Chemical Physics 158 (1991) 221–248
North-Holland

Molecular dynamics study of the photodissociation of carbon monoxide from myoglobin: ligand dynamics in the first 10 ps

John E. Straub [1] and Martin Karplus
Department of Chemistry, Harvard University, Cambridge, MA 02138, USA

Received 24 June 1991

Molecular dynamics simulations are used to study the dynamics of carbon monoxide following its photodissociation from the protein myoglobin. The stochastic boundary approximation is employed for the heme pocket in the presence of solvent. A new three-site model is used for the carbon monoxide that represents its quadrupole moment and includes anharmonic effects in its internal vibrations. The role of the protonation state of the distal histidine and its effect on the dynamics and conformation of the unbound ligand are determined. Analysis of the center-of-mass, rotational and vibrational dynamics of the ligand agrees well with the experimental data of Anfinrud, Han and Hochstrasser [Proc. Natl. Acad. Sci. USA 86 (1989) 8387]. The study seeks to interpret experimental data on the presence of binding sites in the heme pocket (corresponding to both red and blue shifts in the ligand vibrational frequency) which are reached by the ligand soon after dissociation, remain stable for upwards of 1 ns, and whose relative populations are strongly dependent on pH. The possibility that hydrogen bonding of the ligand to the distal histidine may account for ligand vibrational frequency shifts observed experimentally is explored through ab initio frequency calculations. Although the distal histidine clearly is involved, other interactions appear to be required to explain the observed red shifts.

1. Introduction

The photodissociation and rebinding of ligands in myoglobin and hemoglobin has provided much information for the analysis of the dynamics of structural change and energy transfer in proteins. The now classic work of Frauenfelder and co-workers on the rebinding kinetics of photodissociated carbon monoxide in myoglobin as a function of temperature, pH, and solvent provides experimental information on protein dynamics over times that range from picoseconds to milliseconds [1–4]. At room temperature the rebinding of CO can be described mainly by exponential kinetics, but as the temperature is lowered the rebinding kinetics become strongly nonexponential. A wide variety of experimental techniques have been used to study the transition from exponential to nonexponential behavior and the origin of the latter. Dynamic hole burning experiments, for example, have identified inhomogeneous broadening associated with CO rebinding kinetics below a transition temperature [3,4]. The presence of such a transition in the dynamics has been demonstrated through studies of the temperature dependence of incoherent neutron scattering [5,6], Mössbauer spectroscopy [7] and computer simulations [8–10]. The simulations have shown that the transition occurs for a protein studied in vacuum [8,9] suggesting that it involves factors intrinsic to the protein, though the solvent plays a role as well. Information concerning the dynamics of ligand migration through myoglobin has also been obtained from energy minimization and molecular dynamics studies [11–13].

Experimental and simulation data concerning photodissociation have been interpreted in terms of simplified models which relate the protein motions and ligand rebinding to conformational substates [14–16], solvent viscosity [17–19], spatial diffusion [20–22], quasiharmonic motion [23], and spin glass relaxation [24]. Such models have been useful, primarily as a means of suggesting possible factors determining the dynamics (distribution of barriers,

[1] National Institutes of Health Postdoctoral Fellow. Present address: Department of Chemistry, Boston University, Boston, MA 02215, USA.

competing ligand and protein relaxation times, glass transition) or describing the essential dynamics with as few assumptions as possible. However, all the simplified models are empirical and with few exceptions [22] do not attempt to provide a clear correspondence between their parameters and the coordinates of the protein system.

As part of the photodissociation studies, the infrared spectrum of the carbon monoxide stretch has been measured for the ligand bound to the heme (A-states) and dissociated (B-states). The A-states are observed between 20 and 300 K and the B-states have been observed between 5.5 and 100 K [4,25–27]. In the ligated system, Fourier transform infrared spectroscopy has isolated three distinct ligand stretching frequencies, known as the A-states. The frequency shifts are largely independent of pH and temperature, while the widths and areas of the various peaks are sensitive to both pH and temperature above 180 K. From crystallographic data the CO ligand is known to be disordered at 250 K with at least two conformations [26]. More recently, the A-states have been distinguished according to the angle made by the ligand with the heme plane using photoselection with polarized light [28–30]. Values determined for the ligand stretching frequency ν_{CO}, the corresponding angle with the heme plane α, and the preferred range of pH are summarized in table 1. These provide a connection between the kinetic data associated with a particular frequency shift and the ligand conformation. It has been proposed that the A-states correspond to different global conformations of the protein with the A_0-state a precursor in the unfolding transition of myoglobin. However, it is possible that the energy difference corresponds to more local changes in the conformation or to different protonation states of residues forming the heme pocket. This would not contradict the conclusion that the A-states correspond to different substates of the protein since such minima on the multidimensional potential energy surface may be separated by local or more global protein conformational changes [16].

Table 1
Summary of experimental absorption bands of A- and B-states

State	ν_{CO} [a]	pH range [b]	α [c]	Temperature [b]
A-states				
A_0	1966	low	$15\pm3°$	>260K
A_1	1946	all	$28\pm2°$	
A_2	1941			>200K
A_3	1930	high	$33\pm4°$	>260K
B-states				
B_0'	2150			
B_0	2139			
B_1	2131	low		
B_2	2119			<20K

[a] ν_{CO} for CO in the gas phase is 2143 cm^{-1}.
[b] General range of pH or temperature where the population of a given state is most prevalent.
[c] Angle of CO bond with respect to the heme plane [28–30].

The early protein dynamics following photodissociation of myoglobin have been studied using time-resolved femtosecond electronic spectroscopy [32] which shows the formation of the deoxy myoglobin within 350 fs [32,33]. Computer simulations of the photodissociation of CO from myoglobin and hemoglobin have demonstrated a fast iron out-of-plane motion in the range 50–150 fs [34,35] and slower relaxations involving more global conformational changes of the protein over a period of at least 100 ps [35].

Low-temperature infrared spectroscopy of the CO stretching frequency following photodissociation shows three distinct values; all shifted relative to the free molecule [25]. These states of CO are known as the B-states and appear to have a one to one correspondence to the three different A-states; the frequencies are also summarized in table 1.

There has been some success in defining the transient events of ligand photodissociation at room temperature using subpicosecond infrared spectroscopy [36]. These studies have been directed at characterizing the time scale for formation of the B-states of the dissociated CO ligand in hemoglobin. The B-states are observed within 300 fs of bleaching and the spectrum does not change significantly between 300 fs and 1 ns. In accord with the low-temperature experiments, the broad frequency distribution for the dissociated CO at room temperature has been analysed as a superposition of broadened B-states. Up to 50 ns, 85% of the ligand remains in the heme pocket. For photodissociation with radiation at 580 nm, the maximum available energy would be 49.3 kcal/mol. Since the dissociation energy of CO is approximately 23.1 kcal/mol for hemoglobin, the excess energy is 26.2 kcal/mol [37]; for myoglobin a similar value is

expected [37]. Based on the energy separating the excited ($^3T_1$ or $^3T_2$) electronic states involved in photodissociation from the ground (^5E) state of HbCO [38], it was estimated that approximately 16.8 kcal/mol of the energy remains in the heme and 9.4 kcal/mol is in relative translation of Fe and CO. With Fe and CO free, the CO would have a kinetic energy of $[m_{Fe}/(m_{CO}+m_{Fe})]$ 9.4 kcal/mol $\cong$ 6.3 kcal/mol; if the Fe were rigidly bonded in the heme, more than 6.3 kcal/mol would end up in the ligand translation, so the ligand energy should fall in the range 6.3–9.4 kcal/mol. As pointed out by Anfinrud et al. [36], for an energy of 6.3 kcal/mol the ligand initially moves away from the heme at a velocity of 13.6 Å/ps [36]. The unbound CO is observed at 300 fs after dissociation, which is the time resolution of the experiment. Within 300 fs the CO would have traveled 4 Å given the initial velocity of 13.6 Å/ps. From the trajectories the actual Fe–C distance is usually 4–5 Å from Fe, which is typically reached within 100 fs (prior to dissociation the Fe–C distance is approximately 2.3 Å); the longest calculated distance is 7 Å. It has been speculated that the CO would undergo several collisions in this time rendering its motion diffusive [36].

To determine possible binding sites for the ligand CO capable of inducing the frequency shifts observed in the B-states we examine the heme pocket in detail. The heme pocket is rather small and hydrophobic in character. X-ray diffraction data taken at pH 6.0 indicate that a water molecule may occupy the heme pocket in deoxymyoglobin [39], but neutron diffraction data at pH 5.7 show there is insufficient room for both a CO ligand and a solvent molecule [40]. The majority of residues forming the heme pocket are nonpolar or have their polar groups occupied in hydrogen bonding. This is true for all carbonyl and amide backbone groups. The hydroxyl group of Thr 67 and the protonated $N^{\delta 1}$ of the distal His 64 form hydrogen bonds to the solvent. The exceptions are the heme group itself (the polar atoms are Fe ($+0.24e$) and NA, NB, NC, ND ($-0.18e$) and the $N^{\epsilon 2}$ of the distal His 64. The pK of the distal histidine is 5.5 [41]. Two diagrams of the heme and some of the important pocket residues are shown in fig. 1.

It has been proposed that the heme and distal histidine play an important role in inducing the frequency shifts observed in the A- and B-states [42]. Neutron diffraction studies of oxymyoglobin demonstrate the presence of a hydrogen bond between the protonated $N^{\epsilon 2}$ of the distal histidine and the ligand O_2 [43]. In contrast, similar studies of carboxymyoglobin find no evidence for a hydrogen bond between the ligand CO and the distal histidine [40]. This is likely to result from the difference in the charge distribution of liganded CO and O_2, as well as differences in the orientation of CO and O_2 with respect to the heme.

The effect of pH on the heme pocket in the range studied experimentally (pH 5 to 9.5) may be approximated by noting that the most important change is in the distal histidine which would be charged at low pH (<5) and neutral at higher pH (>6.5) since the pK_a is 5.5 [41]. Fig. 2 shows potential energy surfaces for the interaction energy of CO ligated to the heme in the X-ray crystal structure of Kuriyan et al. [26]. Since the maps are based on rigid rotations they are rather approximate. Particularly for the protonated His 64 a displacement is expected (see section 3). We plot nonbonded interaction potential energy contours for the CO molecule ligated to the heme Fe with His 64 (a) protonated and (b) neutral as a function of θ, the Fe–C–O angle, and ϕ, the NC–Fe–C–O torsion [26], where the four nitrogens (e.g., NC) are labelled as in ref. [26]. Although the three-site CO potential function used here (see below) is significantly different from that used in ref. [26], the results for the neutral His 64 are similar. (We note that the three-site CO model was developed for the free CO molecule. Some redistribution of charge in the CO would be expected due to bonding to the heme Fe.) The square at $\phi=60°$ and $\theta=141°$ indicates the placement of the ligand with highest occupancy from the X-ray crystallographic refinement of the structure at pH 6.0 (state C in ref. [26]). As expected the van der Waals contribution is similar for the two pH states. The electrostatic potential is dominated by the protonation state of the histidine and there is a significant change with pH. In the low pH form the ligand is attracted to the protonated $N^{\epsilon 2}$ of His 64 while at neutral pH this region is repulsive.

Assuming the Fe–C bond is perpendicular to the heme plane, the highest occupation state (C) of the X-ray crystal structure of Kuriyan et al. [26] corresponds to an angle $\alpha=51°$; the second most occupied state (D) corresponds to $\alpha=30°$. The energy minimization of the three-site CO model with His 64

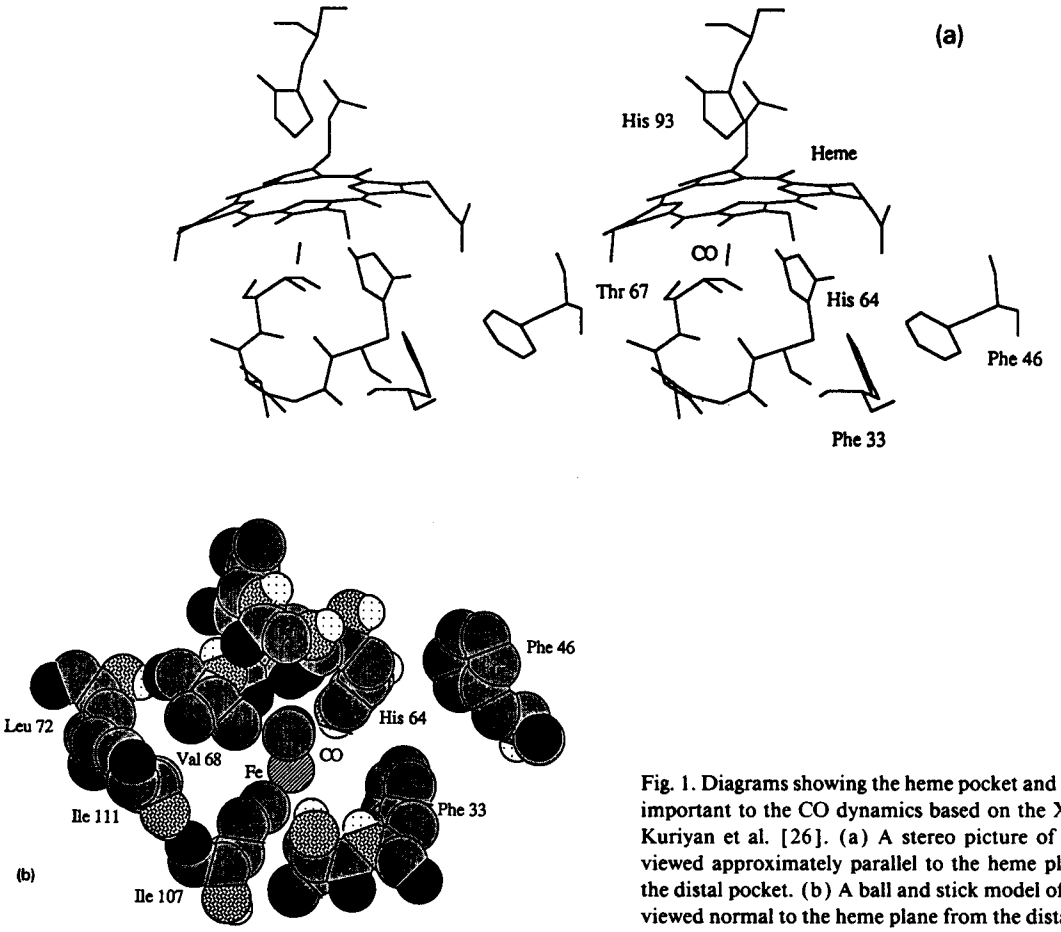

Fig. 1. Diagrams showing the heme pocket and the residues most important to the CO dynamics based on the X-ray structure of Kuriyan et al. [26]. (a) A stereo picture of the heme pocket viewed approximately parallel to the heme plane and showing the distal pocket. (b) A ball and stick model of the heme pocket viewed normal to the heme plane from the distal side.

neutral (high pH) gives a minimum energy configuration with $\alpha = 53°$, and with His 64 charged (low pH) of $\alpha = 33°$. The trend in the experimental data is for the dominant low pH structure to have the smallest $\alpha = 15 \pm 3°$ and the dominant high pH structure to have the largest $\alpha = 33 \pm 4°$ [28]. Thus the calculations for the CO in the potential of the fixed protein predict an α which increases with increasing pH, in accord with the experimental estimates. However, the absolute values of the experimental angle tend to be smaller than those found in the energy minimization.

The above analysis indicates that the effect of high pH on the CO dynamics in myoglobin may be approximated by simulating myoglobin with His 64 charged (low pH) or neutral (neutral pH). A more accurate treatment would allow for dynamic changes in the protonation state and treat the changes in protonation states of titratable residues other than the distal histidine.

In what follows we present the results of molecular dynamics simulations of the short-time behavior of CO after photodissociation from myoglobin with the distal histidine charged and neutral. We first describe the system studied. We make use of the stochastic boundary approximation to isolate the heme pocket region in the presence of solvent. A new three-site model for carbon monoxide is described. It was developed to accurately reproduce ab initio interaction energies with water and various model compounds, the α-CO crystal volume and energy, and the free energy of hydration of CO. The procedure used to generate the initial conditions and run trajectories in the simulation of the photodissociation of CO with the protein having His 64 charged or neutral are outlined. The results and analysis are presented in sec-

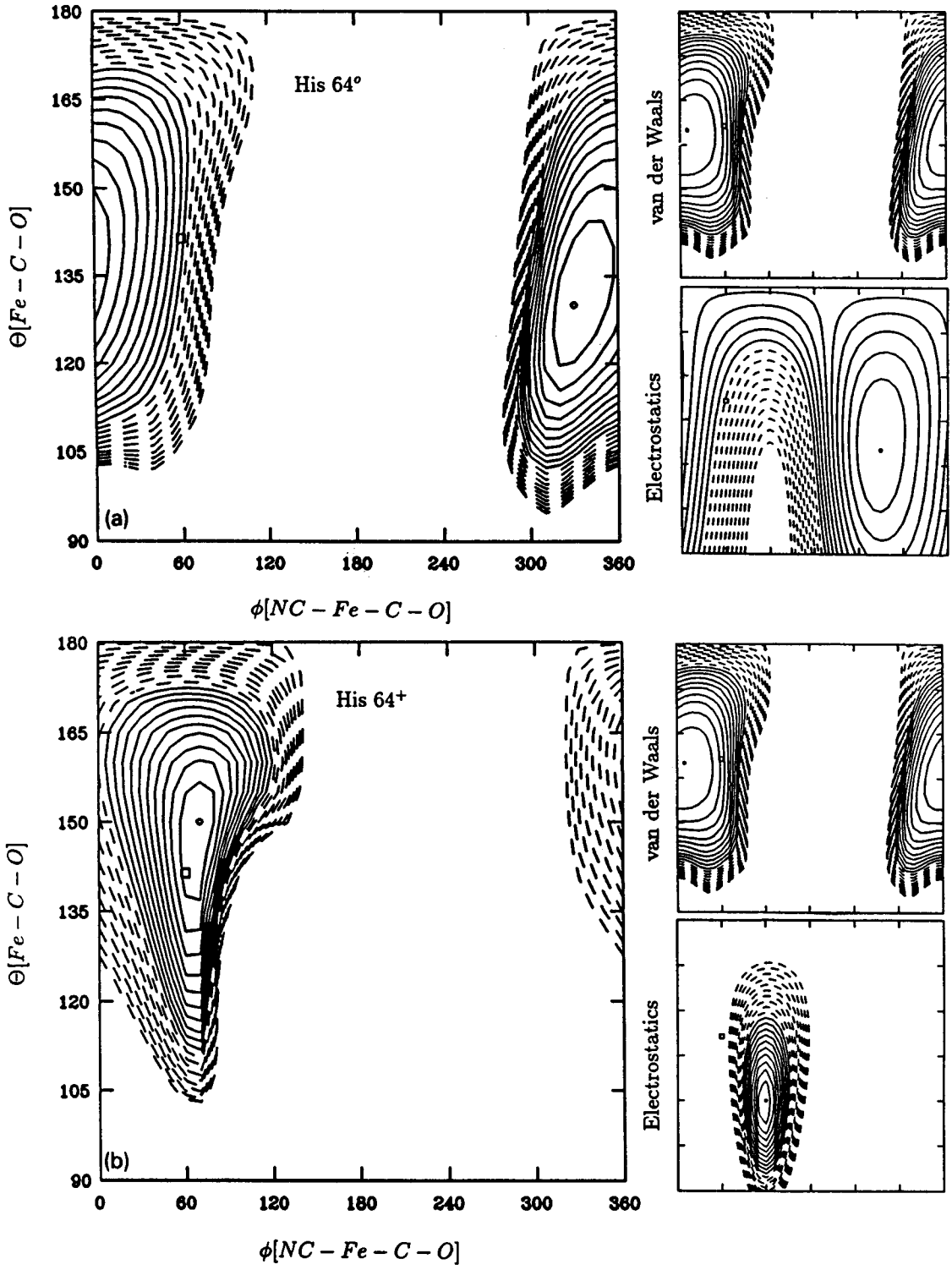

Fig. 2. Potential energy contours for the nonbonded interaction energy of CO ligated to the heme in the X-ray crystal structure of Kuriyan et al. [26] with the His 64 (a) neutral or (b) charged. The square indicates the dominant CO position in the X-ray structure. No energy minimization was performed to relieve strains in the structures with the different protonation states. The separate van der Waals and electrostatic components are shown to the right; the inserts cover the same range of angles as in the main figure. The contours are separated by 1 kcal/mol. The angle θ is defined by the heme iron atom and ligand as the angle Fe–C–O; the torsion angle ϕ is defined as the dihedral angle formed by the atoms NC–Fe–C–O, where NC is one of the heme pyrrole nitrogens (see ref. [26]).

tion 3. A concluding discussion is given in section 4. Details of the studies made to determine the parameters for the CO model are given in the Appendix.

2. Method

Classical molecular dynamics is used to simulate carbon monoxide following photodissociation from the heme group of the protein myoglobin. In addition to the heme group and the CO ligand, the protein atoms making up the heme pocket and the immediate surroundings plus solvent are included in the simulation within the stochastic boundary approximation. This approximation should be satisfactory because comparisons of the X-ray crystal structures for liganded and unliganded myoglobins shows only small differences, except for the change in the heme group and proximal histidine induced by the transition from a planar, 6-coordinate, singlet heme to a domed, 5-coordinate, quintet heme on ligand dissociation. The overall rms difference between deoxy- and carboxymyoglobin for the protein backbone heavy atoms is 0.38 Å and for all nonhydrogen atoms is 1.7 Å. The rms difference between oxy- and deoxymyoglobin X-ray structure is 0.44 Å and 0.74 Å for backbone and all nonhydrogen atoms. These structural differences are comparable with that between oxy- and carboxymyoglobin; the values are 0.43 Å for backbone heavy atoms and 1.74 Å for all nonhydrogen atoms. For the atoms within 16 Å of the heme iron, the rms difference between deoxy- and carboxymyoglobin crystal structures is 0.27 Å for the backbone atoms and 0.8 Å for all nonhydrogen atoms. Moreover, experimental data indicate that after photodissociation the CO molecule remains in the heme pocket for up to 50 ns [36]. Thus, the picosecond simulations of the dissociated CO can be restricted to the behavior of CO in the heme pocket.

In the following subsections, we describe the potential used for myoglobin and a new three-site model for carbon monoxide. The details of the stochastic boundary approximation and the method used for the equilibration and generation of initial conditions for the trajectories are also indicated.

2.1. Protein potential

All calculations employed the CHARMM force field with the version 19 parameter set [44]. Polar hydrogens are treated explicitly and nonpolar hydrogens are treated in the extended atom representation. An exception to this rule is that the ligand is treated by a three-site model, developed for this study and described in detail below. The heme parameters for the deoxy and carbonmonoxy heme group have been given previously [8,26].

The nonbonded van der Waals and electrostatic interactions were truncated by a linear shift function which multiplies the potential and shifts it to zero at the cut-off $r_c = 10$ Å. The shift function is given by

$$S(r) = [1 - 2(r/r_c)^2 + (r/r_c)^4], \quad r < r_c,$$
$$S(r) = 0, \quad r > r_c. \qquad (2.1)$$

This function, or one of similar form, has been shown to provide a satisfactory truncation of the nonbonded interactions in both liquid water [45] and proteins [46]. A recent study of the effects of potential truncation on the simulation of myoglobin determined that a shift truncation gave the most accurate approximation to the dynamics obtained with the untruncated potential [47].

2.2. His 64 protonation state

Simulations of the photodissociation of CO from myoglobin were performed with both charged (low pH) and neutral (neutral pH) forms of distal His 64. Since this study is concerned with the dynamics of CO within the heme pocket, we ignored changes in the protonation state of residues not in the heme pocket [48]. Choice of the δ-protonated tautomer of His 64 as the neutral pH form is based on the neutron scattering structure of Norvell et al. For carboxymyoglobin [40] their data shows that His 64 is neutral at pH 5.7 with $N^{\delta 1}$ protonated and pointing towards solvent and $N^{\varepsilon 1}$ close to the CO. This agrees with the experimental pK (5.5) of the distal histidine for oxycobaltous porphyrin-containing myoglobin, determined by electron paramagnetic resonance spectroscopy [41]. The relative pK_a's of the δ and ε tauto-

mers of His 64 in carboxymyoglobin or unligated myoglobin have not been determined.

2.3. Three-site carbon monoxide model

Carbon monoxide is a diatomic molecule with a small dipole moment (0.11 D), moderate polarizability (3.5 D Å^2), and substantial quadrupole moment (-2.5 D Å). The first molecular dynamics calculations for a molecular liquid were carried out with a Stockmayer model for carbon monoxide consisting of a Lennard-Jones sphere with an embedded point dipole, and an extended Stockmayer model with an embedded point quadrupole [49]. The results showed that the 0.11D dipole moment of carbon monoxide does not contribute significantly to the rotational motion of the CO, which is determined almost entirely by the quadrupole moment. In fact, it was found that the dipole moment must be increased by a factor of ten to mimic correlation resulting from the quadrupole moment [49].

Previous models for carbon monoxide have consisted of Stockmayer models (with point dipole and quadrupole moments) [49] "nonpolar" diatomic modes with small atomic charges (0.021 electrons) approximating the experimental dipole moment but no quadrupole [12,13,34], and a five-site model used in lattice dynamics calculations for solid carbon monoxide [50,51]. We have developed a three-site model which reproduces ab initio interaction energies of CO with CO, water, formamide, methanol, and imidizole, gives an excellent lattice constant and sublimation enthalpy for solid α-CO, yields the hydration free energy of CO, and quantitatively reproduces the vibrational frequencies of CO with an RRKR potential [52]. Details of the fitting procedure and results are given in the Appendix.

The three-site model consists of Lennard-Jones interaction sites and point charges centered on the carbon and oxygen atoms, and a point charge fixed at the molecular center-of-mass. The parameters are given in table 2. The center-of-mass charge, which is massless, couples only to the translational motion of the carbon monoxide molecule and is therefore easily treated in the equations of motion. The force due to an electrostatic field interacting with the CO center-of-mass charge is distributed to the carbon (3/7) and oxygen (4/7) in proportion to the relative masses of carbon and oxygen.

Table 2
Summary of parameters and properties of the three-site model for carbon monoxide

Site	Charge (electrons)	ϵ (kcal/mol)	σ (Å)
C	−0.75	0.0262	3.83
O	−0.85	0.1591	3.12
com	1.6		
Multipole moments	Three-site	Experimental	
μ [a]	0.35	0.112	
$\partial\mu/\partial r$ [b]	0.24	3.1	
$\frac{1}{2}Q_{zz}$ [c]	−2.39	−2.45	
α-CO crystal properties at 8 K	Three-site	Experimental	
lattice constant	5.71	5.646	
unit cell volume	186.2	180.0	
$-E_{\text{sublimation}}$	1.87	1.99	

[a] In units of D.
[b] In units of D/Å.
[c] In units of D Å where z is the direction along the CO bond.

In the CHARMM empirical energy function, the potential for bond stretching is assumed to be harmonic [40]. For the three-site model we employ the anharmonic RRKR stretching potential of Huffaker [52], which was used previously in simulations of CO in liquid Ar [53]. The potential accurately reproduces the CO bond stretching frequency through the energy range examined. The function is displayed in fig. 3 and compares well with the harmonic approximation for vibrational energies less than 5 kcal/mol. The trajectories show that the carbon monoxide molecule is rarely vibrationally excited to more than 3 kcal/mol, while the dissociation energy of CO is 256 kcal/mol (the largest bond energy of any diatomic molecule) [54]. Although the anharmonicity is small, it is included because it has been shown that even small anharmonic contributions can be important in the dephasing of an oscillator, though less so in the energy redistribution [55].

2.4. Stochastic boundary approximation

Stochastic boundary dynamics [56–58] was carried out for the chosen system. The center of the system was chosen to be the ligand carbon atom in the X-ray crystal structure. Atoms within 12 Å of the

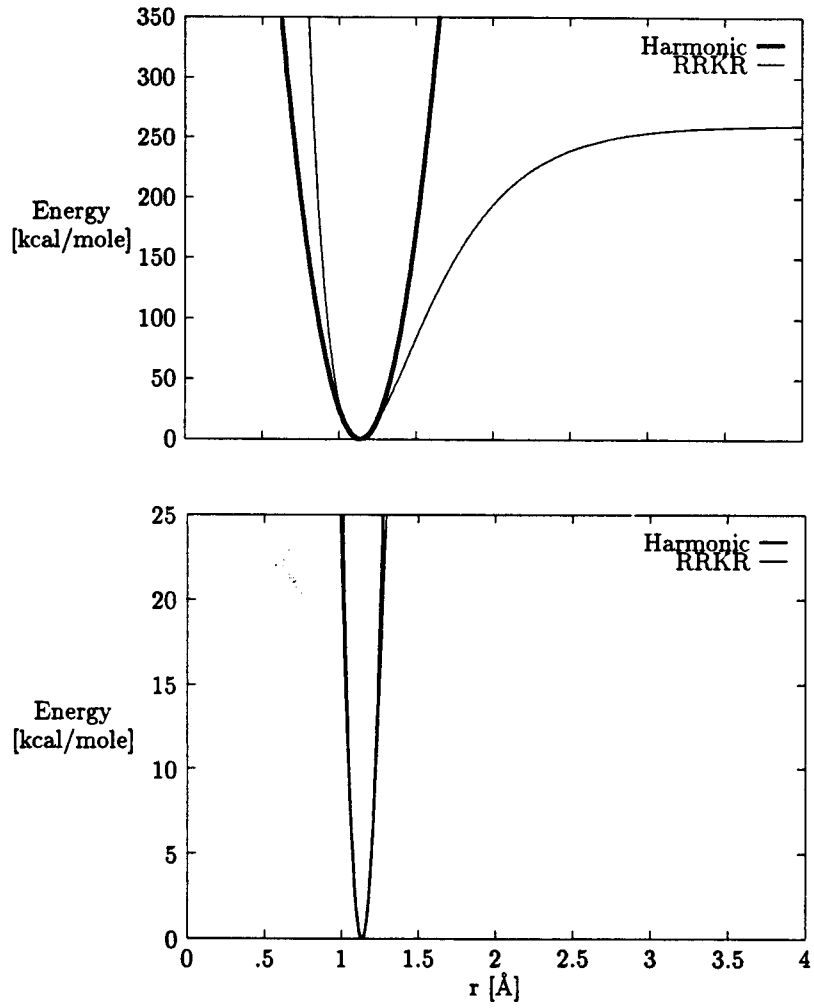

Fig. 3. The CO bond stretching potential for the RRKR potential of Huffaker [52] compared to the harmonic approximation.

center (*active site region*) were propagated according to Newton's equations using the Verlet algorithm and a time step of 1 fs. Nonhydrogen atoms in the volume outside 12 Å and inside 16 Å (*buffer region*) were propagated according to the Langevin equation with harmonic constraints determined from averaged X-ray temperature factors given below [58]. Atoms outside 16 Å (*reservoir region*) were held fixed (but they contribute to the forces on moving atoms). The system used consisted of a total of 1996 atoms: 1487 protein atoms, 48 atoms of the heme group, 153 water molecules and the ligand. At the beginning of the calculation, 1081 atoms were treated with Newtonian dynamics, 334 with Langevin dynamics, while 581 atoms were fixed. During dynamics, solvent molecules may move between the active site and buffer region so that their dynamics (Newtonian or Langevin) will be affected. It has been observed that fixing atoms in the reservior region may overly constrain the motion of protein atoms in the buffer region [58]. Because we are interested in the heme pocket region, we believe that any excess rigidity arising from the fixed atoms of the reservoir region will not adversely affect the results, while electrostatic interactions of the CO with the reservoir region may be important for a realistic description of its behavior (see

also below). The reservior region of fixed atoms consists of residues 1–21, 48–57, 74–87 and 112–153; the remaining protein atoms are included in the dynamics. The heme and residues forming the heme pocket are in the Newtonian dynamics region. The heat bath temperature used was 300 K and the friction constant for protein and water atoms is 62 ps^{-1}. Averaged X-ray temperature factors employed for determining the harmonic constraints were 14 $Å^2$ for backbone, C_α, and sidechain atoms, 15 $Å^2$ for β position atoms, 16 $Å^2$ for γ position atoms, and 17 $Å^2$ for all other atoms.

The constraining force and friction constants for the protein atoms were scaled using a cubic spline function which varied from zero at 12 Å to a maximum of one-half at 14 Å. All bonds to hydrogen atoms were constrained to have fixed length and were propagated using the SHAKE algorithm [59]. Solvent molecules, represented by a modified TIP3P potential [60], were constrained relative to the center of the system by a potential of the Lennard-Jones form at 16 Å [58].

2.5. Initial conditions

The forces on the atoms and their dynamics were calculated using the macromolecular simulation program CHARMM [44]. The equations of motion were solved with the standard Verlet algorithm using a time step of 1 fs. The full protein was used to accurately represent the long-range electrostatic potential in the heme pocket region [61]. Preliminary studies including a reduced protein system led to larger changes in the protein structure and deformation of the heme pocket.

To relieve strains in the X-ray structure the energy of the system was minimized with weak constraints on the protein atoms for 100 steps using the Powell algorithm [62]. A sphere of equilibrated TIP3P water [60] of 18.5 Å radius was overlayed on the X-ray structure with the distal histidine neutral. All solvent atoms within 2.6 Å of a heavy atom and outside 16 Å of the ligand carbon atom were removed. The remaining solvent was minimized for 100 steps to relieve close contacts and equilibrated with 5 ps of Langevin dynamics while the protein was held fixed. The equilibrated 18.5 Å solvent sphere was randomly translated and rotated and the overlay was repeated followed by 5 ps of the Langevin dynamics equilibration of the solvent with the protein atoms under harmonic constraints (with a force constant of 2 kcal/$Å^2$ mol) and 10 ps of Langevin dynamics with a reduced constraining potential (0.5 kcal/$Å^2$ mol). The overlay was repeated a third time and the system was equilibrated with 5 ps of Langevin dynamics with a weak atomic constraint (0.1 kcal/$Å^2$ mol), followed by a final equilibration of 10 ps of Langevin dynamics on the unconstrained system.

The system with His 64 charged was generated from the equilibrated neutral His 64 coordinates obtained after 5 ps of solvent equilibration (with the protein fixed) and 20 ps of equilibration with weak constraints, as described above. The distal histidine was then mutated to its charged form and the full system was equilibrated for an additional 10 ps with no constraints. The resulting system was used as a starting structure for the charged His 64 simulations. In the simulation, the charged His 64 moves outward from the heme pocket and Arg 45 is rotated into the solvent (see section 3).

Ten dissociative trajectories of 10 ps duration were run for His 64 in both the charged and neutral protonation state. The initial conditions for each trajectory were taken from a 45 ps run performed on the two systems starting from the equilibrated structures defined previously. Coordinates and velocities from time points separated by 5 ps on these two trajectories were used. The photodissociation event was simulated by changing the parameters from the carboxymyoglobin system used in the equilibration phase to those of deoxymyoglobin at the beginning of each dissociative trajectory. This consists of instantaneously switching the heme parameters from those for the planar heme with a six-coordinate iron atom to the domed heme with a five-coordinate iron [8]. The bond and angle potential which existed between the heme and ligand in carboxymyoglobin were replaced with standard nonbonded electrostatic and Lennard-Jones interactions between the CO and all atoms of the heme. In each case, the ligand molecule was in a random configuration chosen from the equilibrium trajectory for the ligand bonded to the heme. For the ten trajectories run with His 64 neutral the average orientation of the CO was θ (Fe–C–O) = 151.7 ϕ (NC–Fe–C–O) = 11.7 (range(−30, 38°)) and the R(O–NE2 His 64) distance of 3.07 Å;

with His 64 charged these averages were $\theta = 163.7$, $\phi = 30.8$, R(O–NE2) = 3.37 Å, R(O–HE2) = 3.05 Å. The average value of ϕ with His 64 charged corresponds to eight of ten initial states where ϕ ranged from (−10.3, 71.3). The two remaining trajectories have $\phi = 226.2$ and 203.2; in this case, θ is nearly linear, so that large fluctuations in ϕ are expected. The trend in the average values of θ and ϕ for His 64 neutral and charged agree with expectations based on the potential energy map of fig. 2. The larger average value of both θ and ϕ for CO in the presence of a protonated His 64 agrees with the shift in the electrostatic potential as a result of protonation and a minimum energy which is shifted towards $\phi = 120$ (CO oxygen pointing towards the His 64) and slightly larger θ.

Unlike the recent study of myoglobin by Petrich et al. [35], no special repulsive term was included in the potential for the transition to the dissociated state. This simplification is justified by the energy of the photodissociated ligand. The average initial energy of the photodissociated CO is 8.6 kcal/mol with His 64 neutral and 7.4 kcal/mol with His 64 charged (table 3), which is in good agreement with experimental estimate of 6.3 to 9.4 kcal/mol (see above).

3. Results and analysis

For each trajectory we have calculated the time correlation function for the center-of-mass, rotational and vibrational energies, the rotational reorientation, and the dipole moment. These correlation functions were used to study energy transfer and dynamics. Time series for intermolecular distances between the ligand and heme iron and distal histidine were used to monitor the formation of hydrogen bonding by the dissociated ligand. This data is presented and analyzed in the following subsections. To aid in the analysis, we first describe the structures of the heme pocket for MbCO and for Mb with a neutral and protonated distal histidine (see earlier notes).

In the average protein structure for the 10 ps following photodissociation the mainchain atoms of myoglobin are within 0.23 Å rms of the starting structure. His 64 is found to be much more flexible in the neutral form where the average χ_2 (CA–CB–CG–ND1) = 39.9 with a range (−93.3, 81.7) while

Table 3
Summary of the relaxation of the center-of-mass kinetic energy following photodissociation of the ligand. The value of the kinetic energy is given for the first two maxima in the energy (which always included the global maximum of the trajectory) as well as the energy 1 ps following photodissociation. Energy is given in kcal/mol and time in ps.

Trajectory	Time (ps)	Energy (kcal/mol) maxima	Energy (kcal/mol) at 1 ps
His 64 neutral			
1	0.04	15.13	1.01
	0.20	4.77	
2	0.05	9.97	1.70
	0.50	2.04	
3	0.10	7.67	0.82
	0.60	1.94	
4	0.10	5.61	0.70
	0.45	1.32	
5	0.09	11.13	2.61
	0.40	3.97	
6	0.10	6.63	0.45
	0.55	2.29	
7	0.05	10.66	0.45
	0.30	3.10	
8	0.10	5.55	0.56
	0.20	5.17	
9	0.10	6.10	1.11
	0.25	4.48	
10	0.10	7.25	0.68
	0.25	6.48	
His 64 charged			
1	0.05	10.34	1.52
	0.35	5.32	
2	0.05	6.64	1.02
	0.20	4.95	
3	0.05	4.71	0.91
	0.40	5.74	
4	0.05	10.91	1.47
	0.25	3.26	
5	0.05	4.80	1.44
	0.25	3.59	
6	0.05	9.26	0.67
	0.25	6.95	
7	0.05	7.61	1.28
	0.25	5.12	
8	0.05	5.05	1.66
	0.25	2.35	
9	0.10	6.60	0.26
	0.20	7.03	
10	0.08	7.74	0.04
	0.16	7.60	

for the charged His 64 the average $\chi_2 = 54.7$ with a much narrower range (59.0, 48.8).

We also find a difference in the conformation of Arg 45 in the systems with neutral and charged His 64. The range of initial conformations at the instant of photodissociation and the average conformation following photodissociation are listed in table 4. The dihedral angles χ_2, χ_3 and χ_5 are similar for the two systems, but χ_1 and χ_4 are different. The differences in conformation are established during equilibration and are not altered on photodissociation. The χ_1 (N–CA–CB–CG) dihedral is different by 120° in the two states as is χ_4. The initial range of possible conformations for χ_1 and χ_4 in each protonation state is approximately the same. Our trajectories indicate that the conformation of Arg 45 with His 64 neutral is on average closer to the protein surface due to the distal His being deeper in the heme pocket. The protonated His 64 residue is pushed out from the pocket and the average conformation shows Arg 45 is rotated out into the solvent. Both conformations appear qualitatively similar to the A conformation of Kuriyan et al. [26]. The difference between the A and B conformations in the X-ray data is characterized by changes in χ_1 through χ_5 of 18°, 37°, 161°, 157° and 10° compared to the differences seen between the average Arg 45 configurations with His neutral and charged, which are approximately 120°, 0°, 0°, 120°, and 0° (see table 4).

3.1. Energy transfer

Time series for the vibrational, rotational and center-of-mass kinetic energy were calculated over the full 10 ps duration for each of the twenty dissociative trajectories. The total kinetic energy is

Table 4

	Initial conformation		Average after photodissociation	
	His 64°	His 64⁺	His 64°	His 64⁺
χ_1	(35.4, 79.9)	(−80.5, −42.1)	59.6	−62.7
χ_2	(178.4, −155.7)	(166.4, −165.9)	≈180	≈180
χ_3	(165.6, −160.5)	(162.7, −161.4)	≈180	≈180
χ_4	(69.5, 119.3)	(−173.1, −166.0)	105.5	−151.6
χ_5	(23.2, −7.3)	(19.4, −13.7)	≈0	≈0

$$K = K_{\text{rot}} + K_{\text{vib}} + K_{\text{c.m.}} \tag{3.1}$$

Displayed in fig. 4 is the decomposition of the kinetic energy for four trajectories with His 64 (a) neutral and (b) charged. It can be seen that the time series from the trajectories for the two histidine states are qualitatively similar, though there are quantitative differences, as we discuss in what follows. Trajectories with His 64 neutral (His 64 charged) had average total vibrational energy 0.80 (1.55) kcal/mol, rotational energy 0.82 (1.03) kcal/mol, and center-of-mass translational energy 1.09 (1.11) kcal/mol. These numbers represent the energies averaged over the entire trajectory starting with dissociation and are slightly above the averages expected for CO at thermal equilibrium. At 300 K, $k_B T = 0.59$ kcal/mol and the average equilibrium energies for CO would be: vibration, $k_B T = 0.59$ kcal/mol, rotation, $k_B T = 0.59$ kcal/mol, and center-of-mass translational $3k_B T/2 = 0.84$ kcal/mol. Interestingly, the average vibrational energy is significantly larger in the system with His 64 charged. The more highly excited CO vibrations for the His 64+ system may be correlated with the more linear Fe–C–O angle of conformations at the instant of photodissociation, which is likely to lead to a more compressed CO bond and more effective transfer of energy to the CO vibration.

A collision may be recognized in fig. 4 as an impulsive energy change in the time series of the center-of-mass kinetic energy. From the time series it is evident that the excess initial center-of-mass energy is transferred to the residues of the heme pocket by the first few collisions of the ligand after photodissociation; the decay of the time series suggest that in most cases only two collisions are required. The two peaks of nearly equal height in some of the trajectories indicate that the first collision between the ligand and heme pocket can be elastic; i.e, there is no loss of ligand translational energy on collision. There is no clear difference in the center-of-mass energy relaxation between the trajectories run with His 64 charged and neutral except that the former shows slight coherent oscillations. We discuss these oscillations below.

In table 3 we have listed the values of the components of the initial total kinetic energy, at the maximum, and after 1 ps. The kinetic energy of the ligand is small for the dissociated configuration at zero time

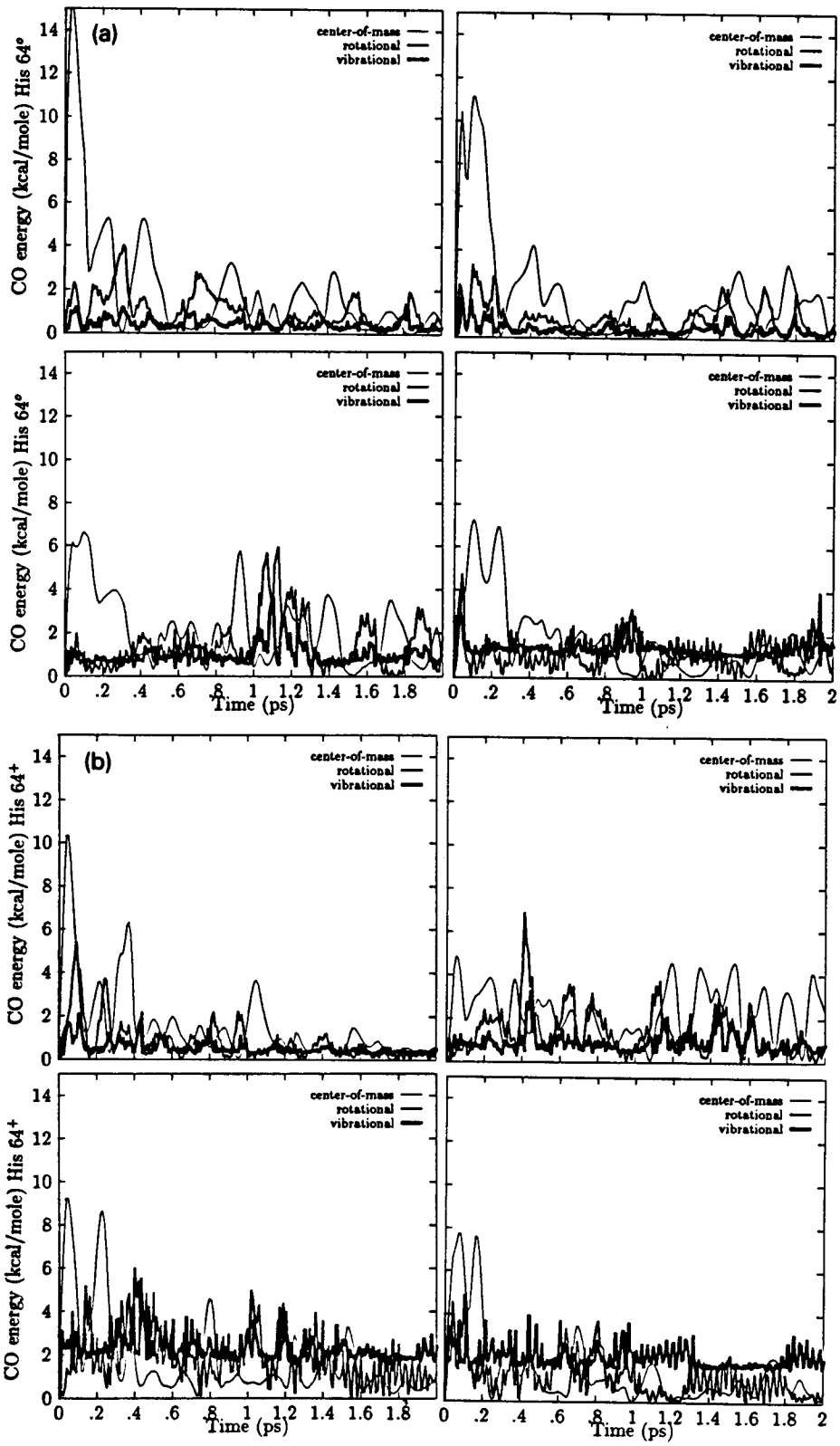

Fig. 4. Time series for the center-of-mass, rotational and vibrational kinetic energy of the CO molecule in the first 2 ps following dissociation for four trajectories with His 64 (a) neutral or (b) charged.

and increases to approximately 10 kcal/mol in the first 0.1–0.2 ps following dissociation due to the CO, heme repulsion. The exact distribution of energy depends on the particular trajectory. However, on average most of the energy (7.4–8.6 kcal/mol) is in center-of-mass translation. The average energy transferred to the CO stretching vibration is approximately 1 kcal/mol, which is small compared to the vibrational level spacing of 6.2 kcal/mol in part because the CO bond length does not change on dissociation in the simulation; the actual distances are 1.12 Å in the Fe–CO complex and 1.128 Å for free CO. The shortness of the CO bond leads to approximately equal repulsive forces on the carbon and oxygen when it is close to the heme. The total CO vibrational energy is nearly constant throughout each trajectory, indicating that there is poor coupling of the CO vibration to the center-of-mass motion, to rotation, or to any vibration in the heme pocket. Interactions with the center-of-mass charge couple only to the CO translation and center-of-mass and not to its rotations or vibrations. The poor V–T transfer can be understood in terms of the adiabaticity parameter. The efficiency of T–V energy transfer may be estimated using the adiabaticity parameter [63]

$$\zeta = t_c / t_v ,$$

where t_c and t_v are the timescales for a collisional event and a molecular vibration, respectively. For a diatomic molecule of vibrational frequency ν, the vibrational timescale is $t_v = 1/\nu$; for the CO frequency of 2143 cm^{-1}, $t_v = 0.015$ ps. The duration of the collision event may be approximated as $t_c = a/v$ where a is the range of the interaction between an atom and the oscillator and v is the relative velocity of the colliding pair. For CO the highest translational velocity is approximately 13.6 Å/ps [35]; if we take 4 Å as the range of the interaction, this result in $t_c = 0.3$ ps. Thus, $\zeta \approx 20$, so that the T–V energy coupling is adiabatic and the resulting energy transfer is expected to be very inefficient since, qualitatively, the protein atom collides with an effectively rigid CO oscillator [63]. The poor V–V transfer can be understood in terms of lack of overlap between the CO stretching frequency ($\nu_{CO} = 2143$ cm^{-1}) and the vibrational density of states of myoglobin (or any protein). There is a nearly continuous density up to about 1200 cm^{-1}, then a window of 400 cm^{-1} up to the carbonyl stretch near 1700 cm^{-1}, and then another window of about 1300 cm^{-1} up to the hydrogen stretching frequencies between 2900 and 3100 cm^{-1}. The latter are not included in the present model because covalent N–H and O–H bonds are treated as fixed. It is possible that a 2:1 (1070 cm^{-1}) or 3:1 (715 cm^{-1}) quantum resonance could provided a mode for energy transfer between the vibrations of the protein and CO stretch. However, there is no evidence in the classical trajectory calculations used here that such a mechanism is active [65]. Long-lived vibrational states are well known from the study of diatomic molecules, such as CO and N_2 in rare gas matrices [64–67]. While the anharmonicity in the CO stretching potential can be important in vibrational dephasing, it is not expected to play a role in vibrational energy transfer when the CO stretch is near the thermal energy.

We have examined the behavior of the center-of-mass and rotational energy using two techniques. In the first, we have averaged the time series for the ligand center-of-mass or rotational energy over the ten trajectories corresponding to each of the two protonation states of the distal histidine. The results are shown in fig. 5a. The center-of-mass kinetic energy relaxes fully within 300 fs of the origin of the trajectory and within 200 fs of the maximum in the energy which occurs at approximately 50–100 fs following dissociation. The rotational kinetic energy shows only moderate excitation. For trajectories run with His 64 neutral the rotational energy has relaxed within 100 fs; when His 64 is charged, the rotational excitation is still weak but longer lived and persists through 300–400 fs. These results are in good agreement with the experimental eximate of 200 fs of Anfinrud and coworkers for CO in hemoglobin.

In addition to the time series averages, which are appropriate for examining relaxation times in nonequilibrium systems, we have calculated the time correlation functions commonly examined for equilibrium events where a sliding time origin is used. In the calculation of the time correlation functions only the last 9 ps of the 10 ps trajectory was used. We justify this approximation by noting the rapid relaxation of the center-of-mass and rotational kinetic energy (within 300 fs) relative to the length of the full trajectory (10 ps), and the near equilibrium average values for the center-of-mass, rotational and vibrational energy of the ligand over the 10 ps trajectory.

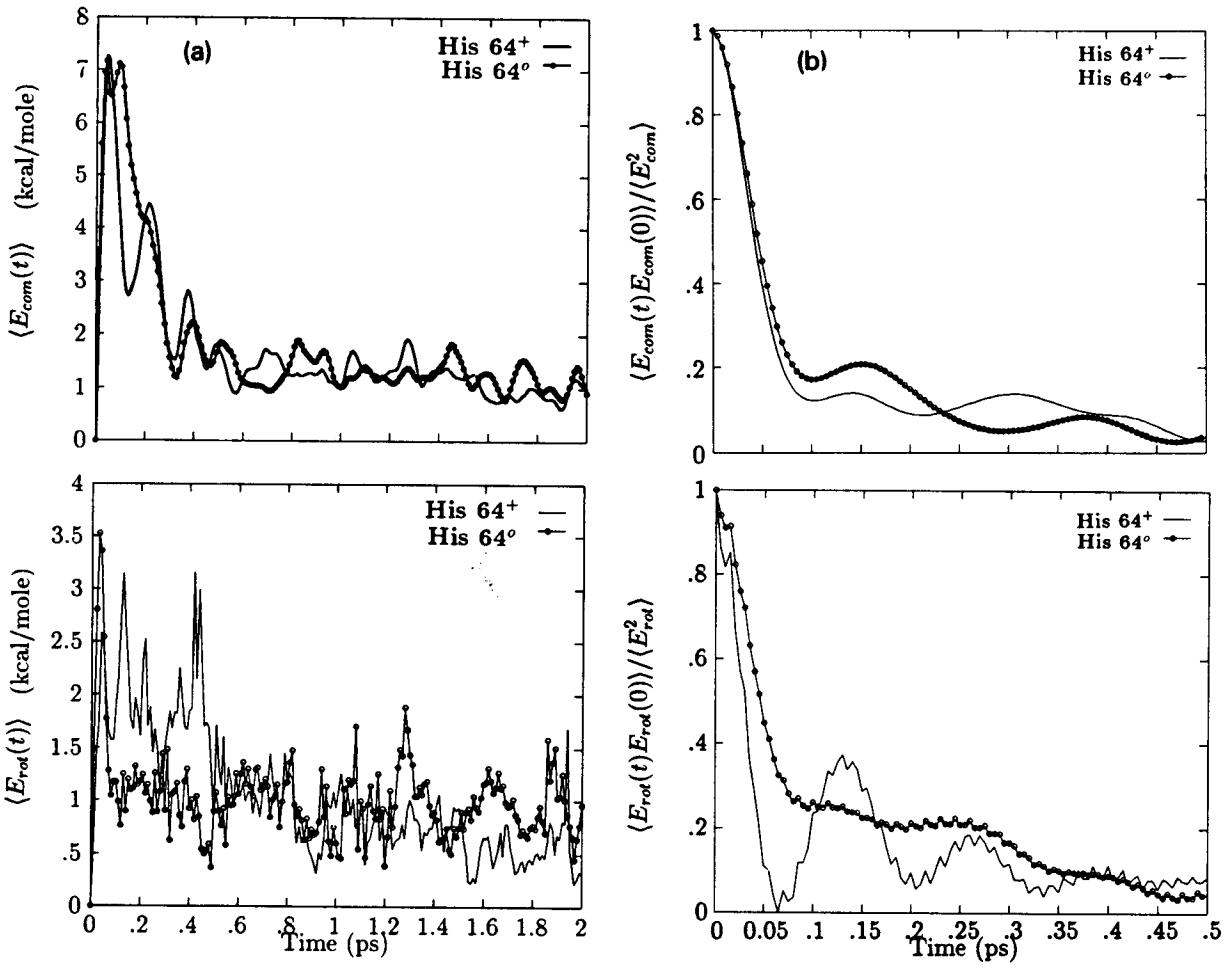

Fig. 5. (a) Time series for center-of-mass and rotational kinetic energy averaged over 10 trajectories with His 64 charged and neutral; (b) the time correlation function of the center-of-mass and rotational kinetic energy of the CO ligand computed for single trajectories from the last 9 ps of dynamics and averaged over 10 trajectories for both His 64 charged and neutral.

The relaxation time to be compared with the experimental results is that of the averaged time series for the nonequilibrium relaxation following photodissociation (fig. 5a).

From the last 9 ps of each 10 ps trajectory, the time correlation function for the center-of-mass energy, $E_{c.m.}$, or the rotational energy, E_{rot}, were determined from the time series according to

$$C_E(t) = \frac{\langle [E(t) - \langle E \rangle][E(0) - \langle E \rangle] \rangle}{\langle [E(0) - \langle E \rangle]^2 \rangle}, \qquad (3.2)$$

where the angular brackets indicate an average over the time series for one trajectory. The rotational energy was calculated by subtracting the translational and vibrational kinetic energy from the total kinetic energy and so includes vibrational rotational coupling. The ten correlation functions for the His system and the His$^+$ system were then averaged. The resulting time correlation function for the center-of-mass kinetic energy is plotted in fig. 5b. We find the correlation time for relaxation of the center-of-mass energy is about 100 fs, in approximate agreement with the experimental estimate of ≈ 200 fs of Anfinrud and co-workers for CO in hemoglobin. The relaxation times derived from the time series averages in fig. 5a are slightly longer, but approximately the same as

those calculated from the correlation functions in fig. 5b. This need not be the case, given the large initial energies due to photodissociation.

The time correlation function for the rotational kinetic energy is plotted in fig. 5b. It can be seen that the relaxation time for the rotational energy is similar to that for the center-of-mass kinetic energy, approximately 100 fs. Although the overall decay behavior is similar for the charged and neutral His 64 trajectories, there is an important difference. The rotational energy correlation function with neutral His 64 is overdamped while that for the protonated His shows underdamped oscillation. This behavior is weaker but still noticeable in the correlation function for the center-of-mass kinetic energy of the protonated His trajectories. These oscillations are due to the rapid formation of a "hydrogen bond" between the protonated His 64 and CO, which leads to hindered rotation of the ligand. The frequency of these oscillations (≈ 0.15 ps) may be determined by the time for the hydrogen bonded ligand molecule to librate as a hindered rotor. If the hydrogen bonding energy imposes a sinusoidal potential on the CO rotation of the form $V = \frac{1}{2} V_0 (1 - \cos 2\theta)$, the corresponding force constant would be 3.4 kcal/mol for this 222 cm^{-1} libration, compared to 0.120 kcal/mol (42 cm^{-1}) for the librational modes seen in liquid carbon monoxide and 1.8 kcal/mol for α-solid carbon monoxide [71]. The oscillatory structure is present, but much weaker, in the trajectories with neutral His 64. We discuss below the nature of the specific interactions.

3.2. Structural analysis

In fig. 6 we display time series for the separation of the ligand and the heme Fe or $N^{\epsilon 2}$ of His 64 for four dissociation trajectories with His 64 charged and neutral. In each figure we plot the distance between the reference protein atom (Fe or $N^{\epsilon 2}$) and both the C (r_C) and O (r_O) of the ligand. The difference in distance between r_C and r_O describes the orientation of the CO relative to the reference atom. For example, if $|r_C - r_O|$ is close to 1 Å the C and O of the ligand and the reference atom are in a nearly linear orientation. This is expected for a hydrogen bond. If $|r_C - r_O|$ is close to 0 Å, the C and O of the ligand are equidistant from the reference atom and in a perpendicular orientation. This is represented schematically in fig. 7. The hydrogen bonding geometry is similar to that of fig. 4b in ref. [42] except that the figure is for unprotonated $N^{\epsilon 2}$; the backbonding geometry is similar to fig. 4d.

The distance of the ligand from the iron atom increases initially (over a few tenths of a ps) and oscillates with a period of 0.5 to 1 ps over most of the trajectory. Rotation is evident in the neutral His trajectory (relative values of Fe–C and Fe–O); in the protonated His trajectory either the O or C seem to be closer to Fe for most of the trajectory (fig. 7). There are instances when the ligand approaches the heme iron to within less than 3 Å; this is to be compared with the equilibrium bonding distance in the carboxymyoglobin system ($r_{Fe-C} = 2.7$ Å).

The distance of the ligand from the distal histidine provides insight into the mechanism of hydrogen bonding. In each of the trajectories with His 64 charged (fig. 6b), there is a close association of either the carbon or oxygen of the ligand with $N^{\epsilon 2}$ within 0.5 to 1 ps and it remains associated for the rest of the trajectory. The distance of the energy minimum for CO from the hydrogen of the protonated imidazole is 2.4 Å for C and 2.2 Å for O, in correspondence with the presence of a relatively weak hydrogen bond (see table 5). We define a "hydrogen bond" when the donor and acceptor heavy atoms are closer than 3.5 Å and the donor hydrogen and acceptor heavy atom are closer than 2.5 Å. Hydrogen bond formation usually occurs within 1 ps of photodissociation following the transfer of energy from the ligand to the protein residues forming the heme pocket. In the time series, this is evident from the small separation of either the C or O atom from $N^{\epsilon 2}$ and the approximately linear orientation of the C–O–$N^{\epsilon 2}$ (approximately 1 Å difference in the C and O distances). Nine trajectories have the C hydrogen bonded and one trajectory has the O hydrogen bonded on average. This is in accord with the relative binding energies shown in table 5.

In the neutral His 64 trajectories the orientation of the CO is usually perpendicular to the heme plane, which corresponds to an approximately in-line orientation of CO and Fe, and perpendicular orientation to the bisector of the $C^{\epsilon 1}$–$N^{\epsilon 2}$–$C^{\delta 1}$ angle of His 64 (equal C and O distances). This arises from the positive charge at the center-of-mass of the CO model, which interacts with the negative $N^{\epsilon 2}$, and corre-

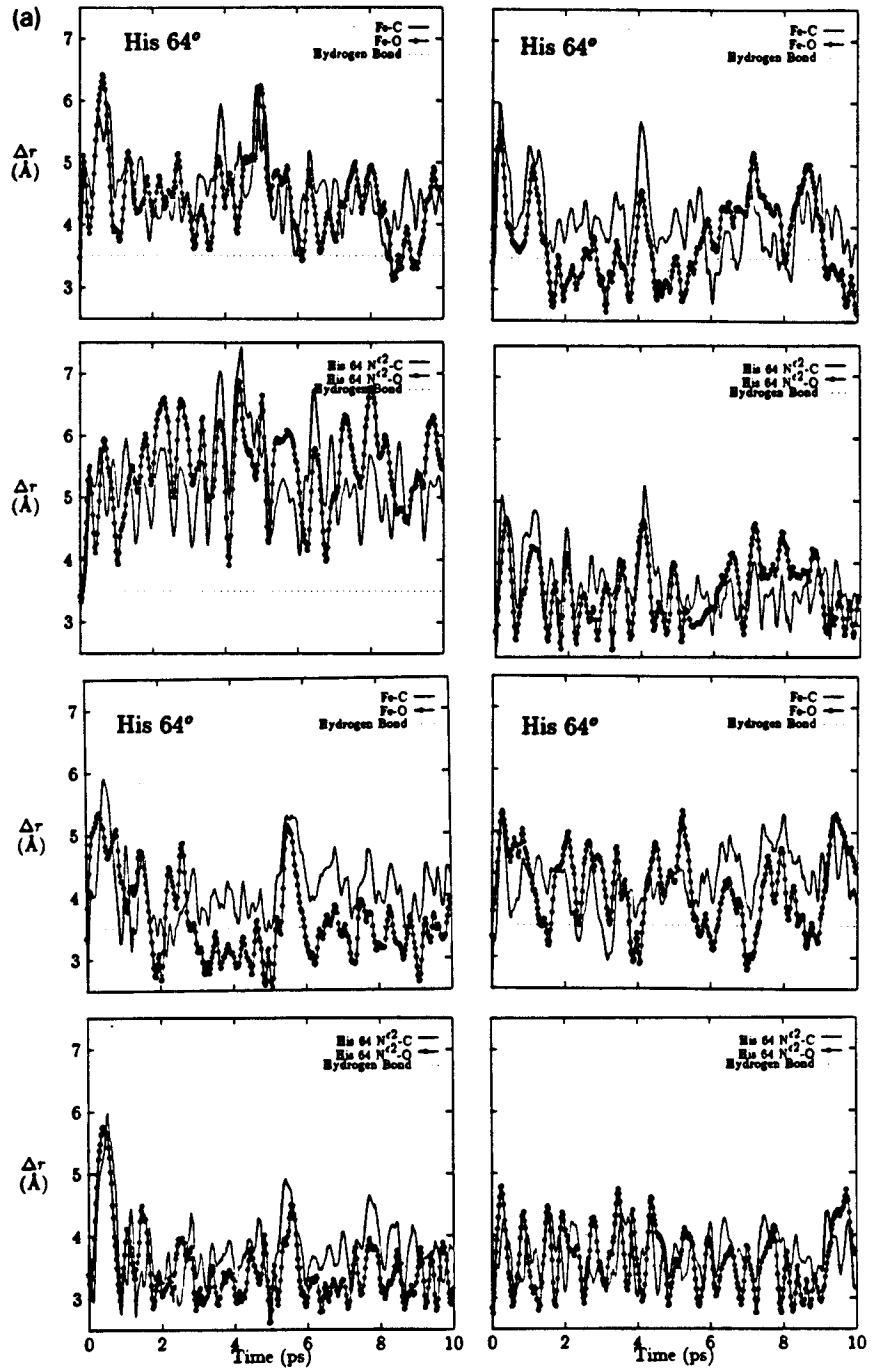

Fig. 6. Time series for the CO–Fe and CO–His 64 distance for four trajectories with His 64 (a) neutral or (b) charged. Distances from the C or O atom to the heme Fe or $N^{\varepsilon 2}$ of His 64 are shown over the 10 ps trajectory. A dotted line is displayed at 3.5 Å indicating the minimum distance criterion for the formation of a hydrogen bond. For a given trajectory the CO–Fe plot is above the CO–His 64 plot.

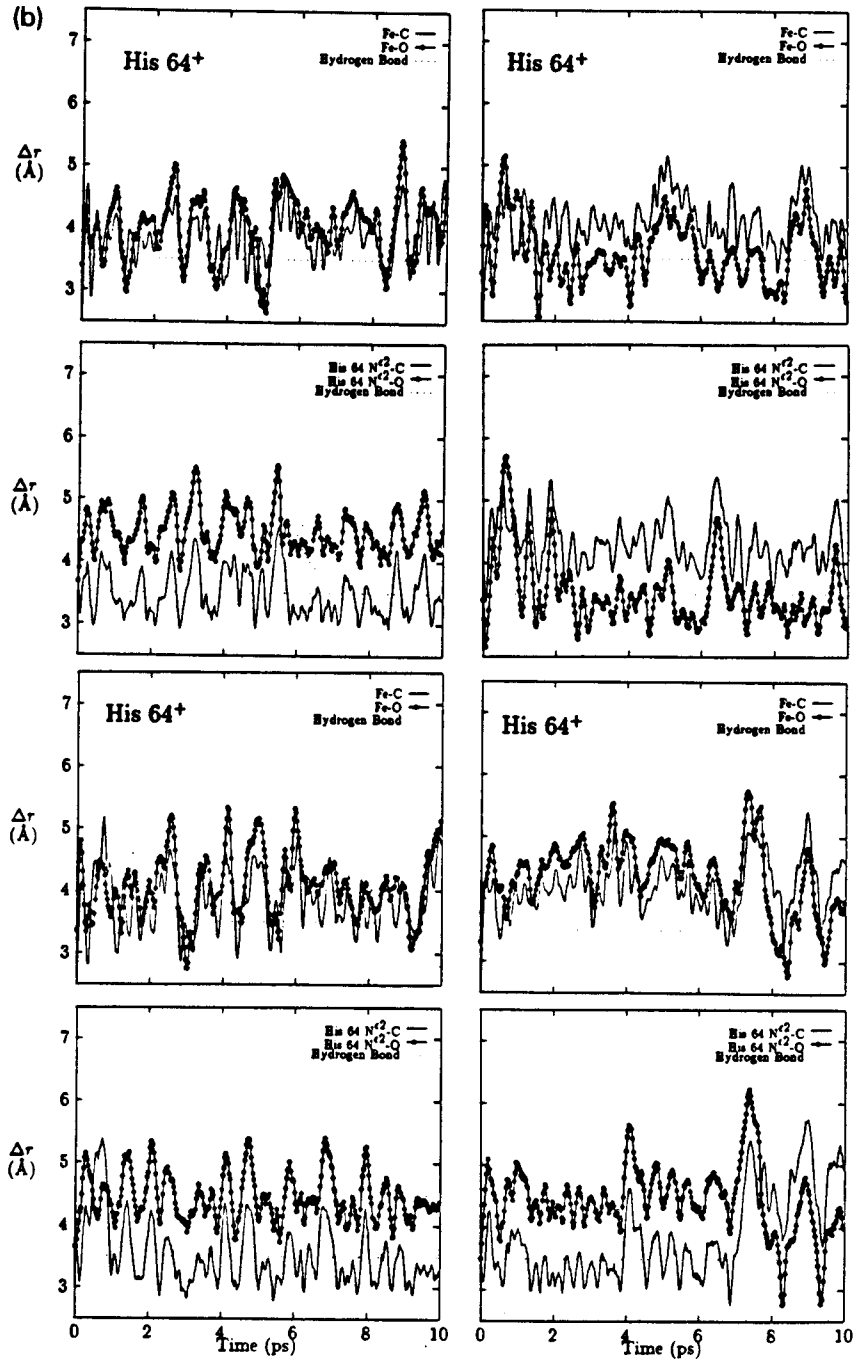

Fig. 6. Continued.

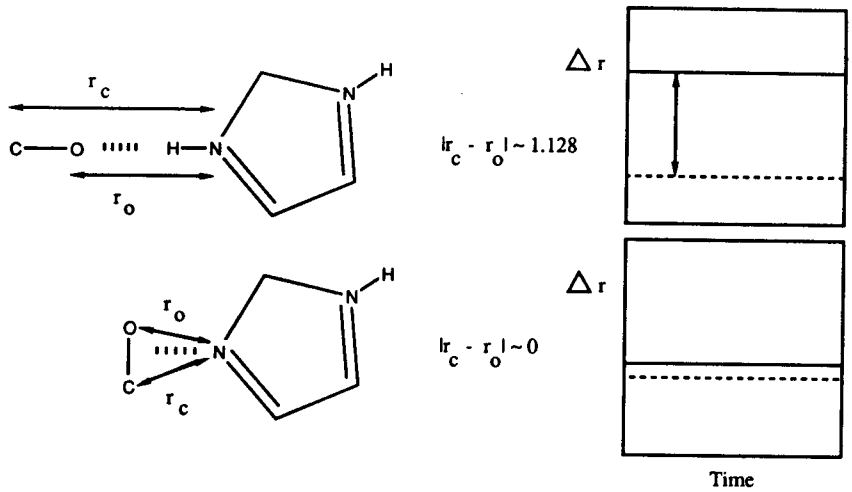

Fig. 7. Schematic diagram showing the orientation of the CO molecule relative to the distal histidine. They correspond to similar (perpendicular back bonding) or different (hydrogen bonding) Δr's for the C and O in the time series of fig. 6.

sponds to a back-bonding configuration. The mean distance of C or O from $N^{\epsilon 2}$ is 3.5–4.0 Å, in agreement with the distance found for the CO–imidizole complex (table 5). Based on the crossing of the C and O to $N^{\epsilon 2}$ distances in the trajectory (fig. 6), there is considerably more rotational motion in this back-bonding configuration than for the linear hydrogen bonding arrangement present in protonated His trajectories. In agreement with these results there is some experimental evidence that the dominant CO species (with a frequency of 2132 cm^{-1}) is oriented nearly perpendicular to the heme plane at room temperature [89].

3.3. Rotational reorientation

With linear response theory, the infrared spectrum is proportional to the Fourier transform of the dipole moment autocorrelation function [68]. When the effect of vibrational and rotational motion on the dipole moment are separable, the dipole moment correlation function can be written as

$$\langle \boldsymbol{\mu}(t)\cdot\boldsymbol{\mu}(0)\rangle = \langle \mu(t)\mu(0)\rangle \langle \hat{\boldsymbol{u}}(t)\cdot\hat{\boldsymbol{u}}(0)\rangle , \quad (3.3)$$

where $\boldsymbol{\mu}$ is the dipole moment vector, μ is its magnitude, and $\hat{\boldsymbol{u}} = \boldsymbol{\mu}/\mu$ is the unit vector describing the orientation of the dipole moment vector $\boldsymbol{\mu}$. It is directed along the CO bond (C^-O^+) and is 0.35 D in magnitude (table 2).

The autocorrelation function of $\hat{\boldsymbol{u}}$, which is related to rotational reorientation, was calculated for each trajectory and the averaged results are displayed in fig. 8 for the charged and neutral His 64 states. We have used the last 9 ps of each 10 ps time series in computing the orientational correlation function. We believe the result is representative of the equilibrium reorientational dynamics due to the rapid energy relaxation in the first 300 fs of the trajectory (see previous section). There is a qualitative difference in the trajectories, as is expected from the analysis of section 3.1 and 3.2. The neutral His 64 trajectories show less hindered rotation and a shorter rotational relaxation time than the charged His 64 trajectories. A plateau is reached in the CO rotational relaxation in 200 fs with charged His 64, corresponding to the formation of a hydrogen bond with the distal histidine. This prevents further rotation of the CO and there is no more decorrelation. The decorrelation is more complete for the neutral His 64 trajectories where the distal histidine–CO has a perpendicular orientation and the rotational motion is not hindered by interaction with the protein.

For both protonation states, the rotational decorrelation is slow and incomplete compared to the gas-phase one-dimensional free rotor correlation function (see fig. 8). Gordon [69] studied the rotational

Table 5
Summary of HF/6-31G* ab initio interaction energies for carbon monoxide and various model compounds compared to empirical energies for the three-site CO model interacting with TIP3P water and methanol, formamide, and imidizole using the version 19 CHARMM parameters [a]

	HF/6-31G*		Three-site model	
	r_{min}	$-E_{min}$	r_{min}	$-E_{min}$
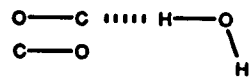	2.56 2.41	1.46 1.23	2.15 2.05	1.80 1.46
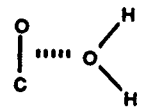	3.29	0.89	3.35	0.87
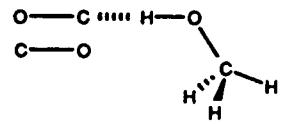	2.54 2.39	1.51 1.23	2.40 2.20	1.56 1.49
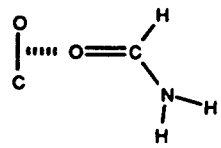	3.25	0.86	3.15	1.29
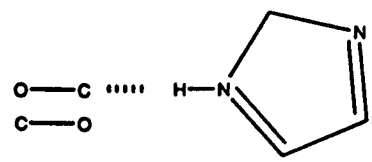	2.58 2.40	1.72 1.50	2.39 2.20	1.75 1.62
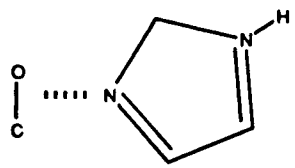	3.46	1.02	3.20	1.28

[a] Distances in Å and energies in kcal/mol. In each case the separation is measured between the oxygen, carbon, or midbond of carbon monoxide and the leftmost atom of the interacting molecule (connected by a broken line).

correlation of CO in many liquid solvents and compared the rotational correlation function extracted from the lineshape of experimental IR spectra with those of strong collision models, or so-called *J*- and *m*-diffusion models. Our results for CO in the neutral His 64 system are similar to those for CO in $CHCl_3$ at room temperature, although rotation in the protein is somewhat more hindered [69].

The free rotor correlation function for the unit vector along the CO bond is simply the rotational corre-

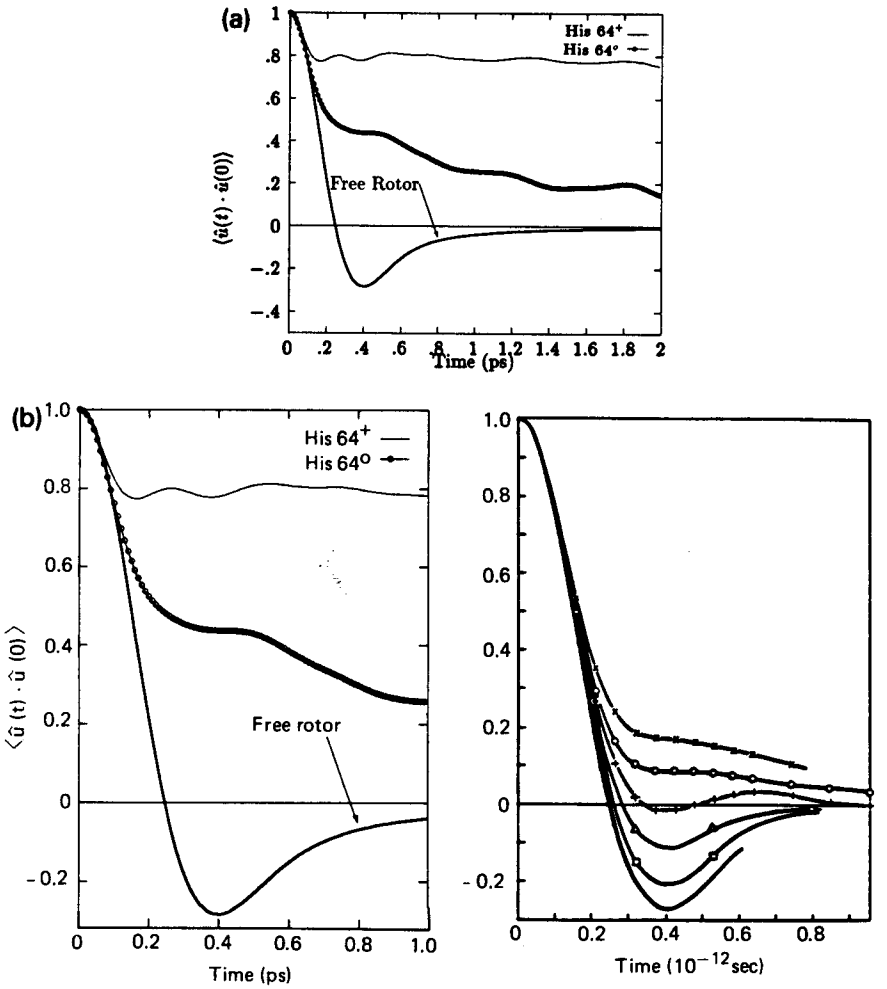

Fig. 8. Time correlation function for (a) orientation of the dipole moment of CO for averages with both charged and neutral His 64 calculated using the last 9 ps of the 10 ps dynamics trajectories and compared with the exact free rotor correlation function. In (b) we compare the result for CO relaxation in myoglobin with that in organic fluids calculated by Gordon for CO in (×) $CHCl_3$, (○) CCl_4, (+) liquid n-C_2H_6, (△) Ar at 510 amagats, and (□) Ar at 270 amagats.

lation function for a free rotor of angular frequency ω averaged over the equilibrium thermal distribution of angular frequencies for a rotor of moment of inertia I (see fig. 8a) [69,70]

$$\langle \hat{\mu}(t)\cdot\hat{u}(0)\rangle = \left[\frac{I}{k_B T}\right]\int d\omega \cos(\omega t)\omega \exp(-I\omega^2/2k_B T)\,. \tag{3.4}$$

The resulting correlation function scales as the average angular rotation time, $\tau_{rot}=(I/k_B T)^{1/2}$, which corresponds to the time scale for the rotational motion of the system. For CO this value is approximately 200 fs ($\tau_{rot}=\sqrt{I/k_B T}=188$ fs for CO at 300 K) in agreement with the rapid initial decay found from the trajectories for both neutral and protonated His 64.

Models for rotational spectra in hindered rotor systems have been used for CO in liquid and solid carbon monoxide [71], as well as in solid Ar matrices [72]. The barrier height for CO rotation can be

determined from these models [71]. It might be possible to determine the mean barrier to rotation of the dissociated CO in the heme pocket through a lineshape analysis by assuming changes in the vibrational frequency contribute to the shift of the line center while the linewidth is due to rotation.

The dipole moment correlation functions derived from experimental spectra for CO in matrices of CCl_4 or $CHCl_3$ show similarities (see fig. 8b) to the hindered orientational correlation function for CO in myoglobin with His 64 charged. In each case the initial decay is close to inertial (as for free rotor), but after 200 fs the function shows a plateau followed by a slow decay. In myoglobin with His 64 neutral the rotation is less hindered and closer in form to an organic liquid. In solid CO and the matrix isolation studies, the hindered rotation is due to a decrease in the volume of the surrounding cage and a corresponding increase in the barrier to CO rotation. The "density" of the protein "solvent" in the myoglobin pocket does not change between the two protonation states; e.g., the van der Waals potential for the CO in fig. 2 is the same with the charged or neutral distal histidine. Thus, the hindered rotation must be due to more specific interactions, the most obvious of which is the formation of a hydrogen bond with the $N^{\epsilon 2}$ proton of the charged His 64.

3.4. Frequency shifts

Experimental evidence, supported by computer simulation, indicates that the B-states of the unbound ligand are formed within 200 fs after photodissociation at room temperature and that they are stable for as long as 1 ns [35]. This indicates that for the simulation times of 10 ps considered here the ligand is expected to remain in the heme pocket, as it does. Experimentally, the B-states are characterized by frequency shifts relative to free CO (2143 cm^{-1}) of up to 24 cm^{-1}; see table 1. Three of the "states" involve red shifts, and one is blue shifted by about 7 cm^{-1} [27]. For CO in benzene matrices at 30 K, red shifts of 10 cm^{-1} have been observed [72]. However, the line is inhomogeneously broadened and the exact value of a frequency shift induced for a single CO is difficult to determine. In Ar at 6 K there is a 4 cm^{-1} red shift [73] while a 5 cm^{-1} red shift is measured for liquid CO at 69 K and solid CO at 59 K [71]. It is unlikely that steric interactions of the type seen in the solvation of diatomics in nonpolar liquids could generate a shift of the magnitude observed in the protein [74]. Dispersion forces are expected to play a role in providing an attractive force capable of inducing a red shift in the CO stretch. However, simple estimates of this contribution suggest that it is too small [75]. This suggests that the electrostatic interactions between the dipole and quadrupole moments of CO and the environment must be involved in the induced shift.

We have performed ab initio vibrational frequency calculations to determine the magnitude of a shift induced in ν_{CO} by the interaction of CO with the imidazole, which is the main polar interaction, in the heme pocket. Hartree–Fock calculations with a 4-21G basis set were carried out on gas-phase CO and for the CO–imidizole complex in three optimized geometries: (1) with the CO bond in line with the H–N bond of a protonated imidizole (hydrogen bonding) and the O pointing toward the imidazole, (2) the corresponding geometry but the C pointing toward the imidazole, and (3) with the CO bond perpendicular to the bisector of the $C^{\delta 2}$–$N^{\epsilon 2}$–$C^{\epsilon 2}$ angle of a neutral imidizole. While there is a systematic error in frequency calculations at this basis set level [76a], we can scale the relative frequencies by use of the expression

$$\Delta\nu_{CO} = \frac{\nu_{CO}^{exp}}{\nu_{CO}} [\nu_{CO\text{-}Im} - \nu_{CO}] , \qquad (3.5)$$

where ν_{CO}^{exp} is the experimental gas phase stretching frequency (2143 cm^{-1}), ν_{CO} is the gas phase frequency for CO calculated with the 4-21G basis set (2301 cm^{-1}), and $\nu_{CO\text{-}Im}$ is the frequency corresponding to the CO stretch in the CO–imidizole complex calculated at the 4-21G level. The results in table 6 show that the hydrogen bond of CO to imidizole can generate a red shift of approximately 17 cm^{-1} while association of the imidizole nitrogen with the π orbitals of the CO can induce a 6 cm^{-1} blue shift. Therefore, a hydrogen bond from the oxygen of the dissociated CO to the $H^{\epsilon 2}$ hydrogen of His 64 is capable of producing a frequency shift similar to that seen experimentally for several of the B-states of CO in myoglobin and hemoglobin. Also, ab initio calculations of frequency shifts in CO–water dimers at the HF/6-31G* level indicate that while a hydrogen bond formed with the CO oxygen pointing toward the hy-

Table 6
Summary of ab initio frequency shifts calculated at the 4-21 G basis set level for ν_{CO} in CO–imidizole dimer complexes.

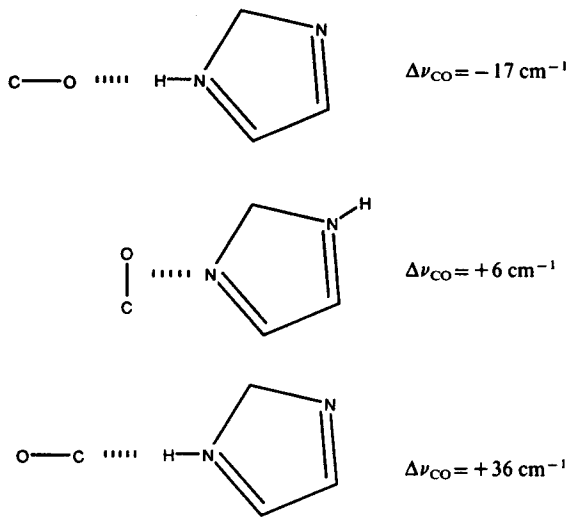

drogen induces a red shift in the CO stretching frequency, a hydrogen bond with the CO carbon pointing toward the hydrogen induces a blue shift of comparable magnitude (see table 6). The results are in accord with recent high level ab initio calculations by Ansburger et al. [76b] for CO in external fields.

The frequency shifts may be understood in terms of the relative stabilization of the four contributing resonance structures of CO [77]. The formation

$$^{+}:C{:}\ddot{O}:^{-} \qquad :C::\ddot{O}: \qquad ^{-}:C:::O:^{+}$$

(a) (b) (c)

of a hydrogen bond to the protonated imidizole using the O of CO as the acceptor stabilizes structure (a) and destabilizes structure (c). This increases the single bond character, weakening the CO bond and inducing a red shift in ν_{CO}. For CO bonding with the C atom as acceptor, the reverse argument applies. The hydrogen bond stabilizes structure (c) while destabilizing (a), leading to a blue shift in the CO stretching frequency. Formation of a back-bonding configuration [78] of CO with the bare nitrogen of imidizole will destabilize structures (a) and (b) which have electrons in orbitals perpendicular to the CO bond, thus increasing the relative importance of resonance structure (c). This leads to an increase in the triple bond character of the CO back-bonded to water, an increase in the bond strength, and a blue shift in ν_{CO}.

4. Concluding discussion

We have developed a model for CO that provides accurate nonbonded interactions with protein residues and used this model for examining ligand energy transfer and dynamics in the first 10 ps following photodissociation at room temperature in myoglobin. The calculated results for energy relaxation are in good agreement with the existing experimental data; i.e., we find the center-of-mass and rotational energy relaxes in ≈ 300 fs and that there is no appreciable vibrational excitation following photodissociation. The orientational correlation function for the ligand shows that the motion is strongly hindered, which is in agreement with the absence of rotational bands in the experimental spectra. Comparison with previous work on CO relaxation in organic fluids shows that the CO dynamics in the heme pocket is similar to that in dense organic liquids such as CCl_4 and $CHCl_3$. We find little or no vibrational excitation of the CO which agrees with the absence of vibrationally excited photodissociated CO in the experiments of Anfinrud et al. [36]. Even for the high initial translational velocity of the dissociated CO, the high frequency of the vibrational motion makes the V–T energy transfer adiabatic and inefficient.

Experimental measurement of the infrared absorption spectra for the A- and B-states shows several distinct frequency shifts at low temperature suggesting that there are discrete interactions in the form of hydrogen bonds or other specific binding sites. Experimental data indicate that the CO molecule remains in the heme pocket for up to 1ns following dissociation. It follows that the B-states are likely to correspond to binding sites or restricted orientations of the CO molecule in the heme pocket. In the present 10 ps simulation all the dissociated CO molecules remained in the heme pocket during the simulation.

The simulations show one dominant dissociated

state for the protonated and the unprotonated histidine; the former involves a C...H–N hydrogen bond and the latter a dative bond between the C=O and the N lone pair. In both cases the predicted shift from ab initio calculations is to higher frequencies, in agreement with simple resonance arguments. The low-temperature experiments do, in fact, show a minor species shifted to higher frequencies (2150 cm^{-1}), relative to free CO, and further this species disappears in the His→Gly mutant [81]. This is in accord with the simulations. However, the fact that the dominant species that are observed have a shift to lower frequencies suggests that there are binding sites, at least at low temperatures, that are not observed in the simulations. It is possible that photodissociation leads to an oriented CO which is "trapped" by the protonated His to form a metastable O...H–N bond that is shifted to lower frequencies according to the calculations. However, this is unlikely for several reasons. Although such trapping is possible (i.e., the binding energy is 1.50 kcal/mol, which would lead to a lifetime of roughly 2.5 ps at room temperature), it does not explain the shift to lower frequencies of the neutral His system (pH 7) nor the fact that the low-frequency species are present in the His→Gly mutant. Frauenfelder et al. [80,81] have done infrared measurements of the dissociated CO species at 10 K at several pH values in native myoglobin and pH 7 in His 64→Gly mutant myoglobin. They find that in native myoglobin there are three states with frequencies at 2150, 2130 and 2119 cm^{-1} at pH 7 and two states at 2130 and 2119 cm^{-1} at pH 5.6. In the His 64 to Gly mutant, the spectra are somewhat broader and only two B states are present (2137 and 2125 cm^{-1}) [81]. At room temperature, which corresponds to the present simulations, the results are not as clear but they appear to be similar to the low-temperature results; i.e., the calculated mean shift from the simulations contrasts with that observed for a CO envelope including the states observed at low temperatures.

The observed red shift contrasts with that found for CO hydrogen bonding to a donor such as water and phenol which has been studied in matrix isolation experiments. At cryogenic temperatures it is typical to see a blue shifted CO stretching frequency, indicating that the carbon atom is acting as the hydrogen bond acceptor [79]. We have carried out ab initio calculations of water–CO dimer systems constraining the O–C–H or C–O–H angle to 180° and found that at the HF/4-21G level the CO–HOH dimer is most stable while at HF/6-31G* through MP4/6-31G* the OC–HOH dimer is most stable in agreement with experiment.

A possible explanation of the absence of a red shift in the simulation of myoglobin is that sites for CO binding are missed due to shortcomings of the force field employed for the protein and the heme. Most important is the extended atom approximation used for the hydrogens linked to carbons of the phenyl groups and possibly those of the heme pyrrole rings. It is well known that, in analogy to the present CO model, the "nonpolar" benzene molecule is highly polar with a large quadrupole moment. This is not present in the extended atom model with which the calculations were done. Instead of neutral united (CH) "atoms", an all-atom force field that has been developed has the CH moiety with a positive partial change on the hydrogen and a negative partial charge on the carbon to yield an overall quadrupole moment of 3.6 D Å for benzene [82]. It is likely that a CO datively linked to benzene will be red shifted; in fact, in the anisole–CO complex the CO frequency is 2137 cm^{-1} [79]. Thus, we suggest that phenylalanine complexes with CO are the source of the red shift, though it is possible that similar interactions with the heme are involved. There are two phenylalanines in the heme pocket (see fig. 1) of which Phe 33 is the most likely candidate. To test this suggestion, molecular dynamics simulations with an all-hydrogen model for myoglobin are being made. Also, ab initio and semiempirical quantum mechanical calculations to quantitate the CO interaction with benzene and the resulting frequency shift are in progress. It would be of great interest in this regard to do low-temperature infrared measurements on Phe 33→Ala, a mutant which has been prepared for kinetic studies.

Acknowledgement

We thank Kryzstof Kuczera, Benoît Roux, Ron Elber, and David Hsu for discussions and Alexander Mackerell Jr. for assistance in carrying out the vibrational calculations for the CO–imidizole dimer. We thank Charles Brooks for helpful comments on cor-

relation functions. We are grateful to Cray Research for making time available to do some of these ab initio calculations. All dynamics calculations were performed on a Silicon Graphics 4D/240. The work was supported by the National Science Foundation and the National Institutes of Health. JS was an National Institutes of Health postdoctoral fellow.

Appendix. Three-site CO model interaction parameters

In this appendix we present the details of the parameterization and testing of the three-site potential model for carbon monoxide used in the simulations. The three-site model consists of Lennard-Jones sites and point charges on the carbon and oxygen atoms and a point charge at the center-of-mass. The charges were first estimated to give approximate agreement with the experimental dipole and quadrupole moments. We then simulated the α-CO crystal structure and adjusted the van der Waals radii and charges to give agreement with the experimental lattice constant and sublimation energy for the crystal. The changes were then refined to fit ab initio quantum mechanical energies for CO interacting with water. Finally, the hydration free energy of the three-site model was calculated and compared with the experimental value.

The point charges correspond to a dipole moment of 0.33 D (C^-O^+) which is slightly larger than the experimental value of 0.11 D. The quadrupole moment of −2.39 D Å calculated about the center of the bond as origin is close to the most reliable experimental estimate of −2.45 D Å, and a recommended value of −2.5 D Å based on experimental and ab initio data [82]. Also, simulations of a modified Stockmayer model for CO (a Lennard-Jones atom with point quadrupole) determined that a quadrupole moment of −2.43 D Å gave a mean-square torque close to that derived from experiment [49].

The experimental dipole moment derivative of CO is 3.1 D/Å [83]. This is substantial considering that the dipole moment is only 0.11 D and a displacement from equilibrium in the CO bond length of only 0.03 Å can change the sign of the dipole moment. Within the atomic nuclear point charge model it is not possible to reproduce the dipole moment derivative without changing the charges as a function of the internuclear distance. The three-site model with fixed charges predicts a dipole derivative of only 0.24 D/Å. However, if the dipole moment is desired for an accurate calculation of the vibrational spectrum to a good approximation one may ignore the dipole derivative during the dynamics but add it as a correction when calculating the dipole autocorrelation function from the trajectory for the CO bond stretch. This was done in the simulation of CO in argon studied by Berends and Wilson [53]. We assume that this is reasonable for CO in the strongly polar environment of a protein, because the dipole moment is small and does not contribute substantially to the CO dynamics.

Anharmonic RRKR stretching potential

The stretching potential employed for the CO ligand is that of Huffaker [52]. The potential has the form of a perturbed Morse oscillator

$$V(r) = V_e(y^2 + b_4 y^4 + b_5 y^5 + b_6 y^6 + b_7 y^7 + b_8 y^8) ,$$

where $y = (1 - e^{-q})$ and $q = 2.697304(r - r_{eq})/r_{eq}$ with r in Å and $r_{eq} = 1.128$ Å, the equilibrium bond length of CO. The equilibrium dissociation energy is

$$D_e = V_e(1 + b_4 + b_5 + b_6 + b_7 + b_8) ,$$

where $V_e = 239.61$ kcal/mol. The coefficients of carbon monoxide are $b_4 = 0.036067$, $b_5 = 0.017505$, $b_6 = 0.014945$, $b_7 = 0.010770$, and $b_8 = 0.008142$ so that $D_e = 260.55$ kcal/mol [52]. D_e is the dissociation energy with the zero-point energy included.

α-CO crystal minimization

We tested the three-site CO potential in the α-CO crystal structure. Fracassi and co-workers have examined the lattice dynamics of this crystal and developed a five-site CO model to fit the lattice vibrations and sublimation energy. The three-site model was used to simulate the CO crystal by minimizing the potential energy with a variable lattice constant. Group truncation was introduced with the cubic switching function given by

$$S(r)=1, \quad r \leqslant r_{on},$$

$$S(r)=\left[\frac{(r_{off}^2-r^2)^2(r_{off}^2-3r_{on}^2+2r^2)}{(r_{off}^2-r_{on}^2)^3}\right],$$

$$r_{on}<r\leqslant r_{off},$$

$$S(r)=0, \quad r>r_{off}, \tag{A.1}$$

for an atom interacting with a group of atoms whose geometric center is a distance r away. In eq. (A.1) $r_{on}=8$ Å, $r_{off}=12$ Å, and the switching function is centered at the geometric center of the group. We fit the lattice constant predicted by our model for the 0 K structure to the lattice constant of the 8 K crystal structure by adjusting the van der Waals radii for the carbon and oxygen atoms. The predicted lattice energy is 2.01 kcal/mol, using the correction of 0.5 kcal/mol for the zero-point energy [50,51]. This is to be compared with the experimental value of 1.92 kcal/mol. These data are summarized in table 2.

Interaction energies

With the point charges fit to give good agreement with the multipole moments of CO, and the Lennard-Jones parameters fit to give a good estimate of the lattice constant for the α-CO crystal structure, we tested our model against ab initio Hartree–Fock calculations with the 6-31 G basis set of the Gaussian 86 program. The results are displayed in table 5. The interaction energies of the CO–water dimer were used to fine-tune the CO charges from those originally determined from multipole moments and ab initio data. We employed a slightly modified TIP3P model for water [60] and used the standard Lennard-Jones combination rules. The final charges for CO were altered by $0.05e$ from the values obtained earlier (-0.8, $+1.7$, -0.9) by fitting to the multipole data and lattice constant of the α-CO crystal structure.

Analysis of the ab initio interactions provides insight to the nature of CO interactions with the protein functional groups. The CO molecule forms weak hydrogen bonds to water with the carbon or oxygen acting as the acceptor atom, with the OC...H–O bond stronger than the CO...H–O bond. The model has a larger charge at the oxygen atom ($-0.85e$), and a slightly smaller Lennard-Jones radius (3.1 Å) relative to that for carbon (3.8 Å) which has a smaller point charge ($-0.75e$). In spite of this the O–C...H–O bond is stronger than the C–O...H–O bond because the oxygen atom is closer (by 0.16 Å) to the large positive charge at the center-of-mass. Also, CO forms a weak but favorable interaction through back-bonding [78] with the π anti-bonding orbitals of the CO molecule. This effect is approximated through the large positive charge ($+1.6e$) at the center-of-mass that yields the correct quadrupole moment. The resulting point charges are similar to those of Hoinkis et al. based on fitting ab initio interaction energies for the CO dimer [31].

As a test of the transferability of the parameters of the CO potential with the protein potential we examined the interaction energies for CO interacting with water, formamide (protein backbone), methanol (threonine) and imidizole (histidine). These interactions were determined to be the most important for CO dynamics in the heme pocket of myoglobin (see previous discussion). The results are summarized in table 5. In all cases, the three-site model gives good to excellent agreement with the ab initio predictions. For hydrogen bonding interactions, the complex involving the carbon is always more stable than that with oxygen. The minimum energy configuration of each dimer predicted by the three-site model is consistently 0.2–0.3 Å shorter in distance and 0.2–0.3 kcal/mol stronger in energy than the ab initio values. A scaling factor may be determined from the ratio of the ab initio energy for the water dimer to the empirical energy for the water dimer. This scaling factor is approximately 0.86 for the HF/6-31G* basis set and the modified TIP3P model [84]. Distances and energies for empirical interactions which are shorter and stronger than the HF/6-31G* results are consistent and systematic. Jorgensen and co-workers have found similar rules in the derivation of the OPLS empirical force field where enthalpies and volumes for liquid state calculations are fit to the experimental data [85].

Hydration free energy

Using the free energy simulation method [86] we calculated the hydration free energy of CO using the three-site model. The BOSS Monte Carlo program was used with a system size of 265 water molecules

run at a constant pressure of 1 atm and constant temperature of 298 K. The box size was approximately a 20 Å cube. We first calculated the free energy of hydration for a methane-like Lennard-Jones sphere and then the difference in hydration energy between the methane-like sphere and CO. The parameters of the methane-like sphere had a diameter 3.8 Å and a well-depth of 0.20 kcal/mol. We used a modified TIP3P water model with a solvent–solvent and solvent–solute cut-off of 8.5 Å. We sampled 5×10^6 configurations for equilibration and 10^6 configurations in averaging for each value of the perturbation parameter λ. We typically found an acceptance ratio between 40 and 50%.

In the first step of the calculation, the hydration free energy of the methane-like sphere was calculated by scaling the radius and well-depth linearly with λ. In the second step, involving the transformation of CO to a sphere, we scaled linearly (1) the distance between C and O and the center-of-mass (where the sphere was centered), (2) the charges on the C, O and center-of-mass and (3) the Lennard-Jones diameter and well-depth for C and O.

The overall hydration free energy for our CO model was calculated to be 2.7 kcal/mol compared to the experimental value of 2.2 kcal/mol [87]. The level of agreement is within the accuracy of the calculation. The details of the calculations are given in tables 7 and 8.

Table 7
Simulation results for Monte Carlo calculation of the difference in the free energy of hydration ΔG_{hyd} between a methane-like Lennard-Jones sphere and nothing with averaging over 1.0×10^6 configurations. The subscripts i and j represent the initial and final values of the perturbation parameter where 0.0 is methane-like sphere and 1.0 is null. The uncertainty associated with the free energy determined for each step $i\rightarrow j$ is calculated as the variance of the distribution of individual averages contributing to the final $\Delta G_{i\rightarrow j}$. ΔG_{ave} is the sum of the forward and backward steps $i\rightarrow j$. Double wide sampling is used

i	j	$\Delta G_{i\rightarrow j}$	$\Delta G_{j\rightarrow i}$	ΔG_{ave}
0.0	0.1	−0.417±0.074	0.145±0.058	−0.281
0.1	0.2	−0.008±0.008	0.685±0.087	−0.346
0.2	0.3	−0.462±0.072	0.529±0.127	−0.496
0.3	0.4	−0.723±0.169	0.882±0.108	−0.802
0.4	0.5	−0.631±0.107	0.121±0.093	−0.376
0.5	0.6	−0.085±0.056	0.240±0.031	−0.162
0.6	0.7	−0.186±0.066	0.383±0.093	−0.285
0.7	0.8	−0.535±0.165	0.241±0.030	0.388
0.8	0.9	−0.066±0.045	0.094±0.019	0.080
0.9	1.0	−0.009±0.002	0.045±0.014	0.018
0.0	1.0	−3.104±0.296	3.365±0.242	−3.234

Table 8
Simulation results for Monte Carlo calculation of the difference in the free energy of hydration ΔG_{hyd} between our three-site model for carbon monoxide and a methane-like Lennard-Jones sphere with averaging over 1.0×10^6 configurations. See calculation details given in the caption of table 7

i	j	$\Delta G_{i\rightarrow j}$	$\Delta G_{j\rightarrow i}$	ΔG_{ave}
0.0	0.125	−0.238±0.138	1.142±0.266	−0.690
0.125	0.25	−0.764±0.080	0.584±0.189	−0.674
0.25	0.375	−0.595±0.143	0.714±0.166	−0.655
0.375	0.5	−0.333±0.057	0.565±0.054	−0.449
0.5	0.625	0.823±0.084	−0.498±0.063	0.661
0.625	0.75	0.710±0.149	−0.821±0.088	0.765
0.75	0.875	0.908±0.160	−0.693±0.089	0.800
0.875	1.0	1.345±0.088	0.136±0.108	0.605
0.0	1.0	1.856±0.334	1.129±0.410	0.363

In fig. 9 we show that the radial distribution functions for the H and O of water are correlated with the C, O and center-of-mass sites of CO for a simulation of a single CO molecule in water. We used a solvent–solute cut-off of 8.5 Å and the radial distribution function is accurate up to approximately 7.5 Å. There

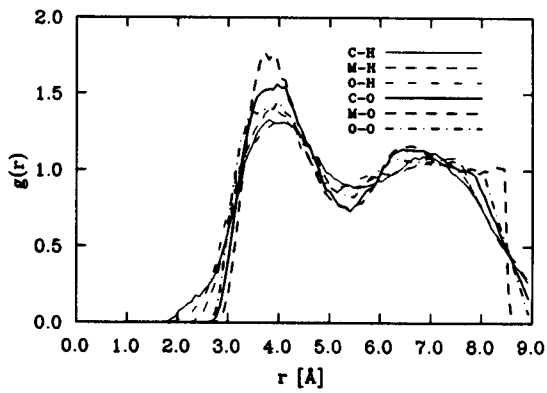

Fig. 9. Radial pair distribution functions for the C, O and center of mass M of carbon monoxide with the H and O of water for a single CO molecule in 265 water molecules. In the figure legends, the leftmost letter refers to the atom of the CO molecule and the rightmost letter refers to the atom of the water molecule. The distribution functions are averaged over 1×10^6 Monte Carlo configurations.

is a strong first peak occurring at 3.8 Å correlating the center-of-mass of CO with the O of water. The distance is in good agreement with the minimum energy distance for the oxygen–midbond interaction 3.4 Å for the CO–water dimer (see table 5). The first peaks for all interacting pairs occur between 3.8 and 4.0 Å suggesting the excluded volume of the CO molecule in water is approximately equivalent to a sphere of diameter 4.0 Å. This is in good agreement with estimates based on the second virial coefficient for CO [88]. Finally, there is a small but significant probability near 2 Å of the H of water interacting with C or O of CO indicating the presence of weak hydrogen bonding of water to CO.

References

[1] R.H. Austin, K.W. Beece, L. Eisenstein, H. Frauenfelder and I.C. Gunsalus, Biochemistry 14 (1975) 5355.
[2] A. Ansari, J. Berendzen, D. Braunstein, B.R. Cowen, H. Frauenfelder, M.K. Hong, I.E.T. Iben, J.B. Johnson, P. Ormos, T.S. Sauke, R. Scholl, A. Schulte, P.J. Steinbach, J. Vittitow and R.D. Young, Biophys. Chem. 26 (1987) 337.
[3] P.J. Steinbach, A. Xie and R.D. Young, submitted to Science.
[4] B.F. Campbell, M.R. Chance and J.M. Friedman, Science 238 (1987) 373.
[5] W. Doster, S. Cusack and W. Petry, Nature 337 (1989) 754.
[6] J. Smith, S. Cusack, B. Tidor and M. Karplus, J. Chem. Phys. 93 (1990) 2974.
[7] F. Parak and E.W. Knapp, Proc. Natl. Acad. Sci. USA 81 (1984) 7088.
[8] K. Kuczera, J. Kuriyan and M. Karplus, J. Mol. Biol. 213 (1990) 351.
[9] J. Smith, K. Kuczera and M. Karplus, Proc. Natl. Acad. Sci. USA 87 (1990) 1601.
[10] D. Case and M. Karplus, J. Mol. Biol. 132 (1979) 343.
[11] R.J. Loncharich and B.R. Brooks, J. Mol. Biol. 215 (1990) 439.
[12] J. Kottalam and D.A. Case, J. Am. Chem. Soc. 110 (1988) 7690.
[13] R. Elber and M. Karplus, J. Am. Chem. Soc. 112 (1990) 9161.
[14] R.D. Young and S.F. Bowne, J. Chem. Phys. 81 (1984) 3730.
[15] A. Ansari, E.E. Dilorio, D.D. Dlott, H. Frauenfelder, I.E.T. Iben, P. Langer, H. Roder, T. Sauke and E. Shyamsunder, Biochemistry 25 (1986) 3139.
[16] R. Elber and M. Karplus, Science 235 (1987) 318.
[17] D. Beece, L. Eisenstein, H. Frauenfelder, D. Good, M.C. Marden, L. Reinisch, A.H. Reynolds, L.B. Sorensen and K.T. Yue, Biochemistry 19 (1980) 5147.
[18] W. Doster, Biophys. Chem. 17 (1983) 97.
[19] P. Hanggi, J. Stat. Phys. 30 (1983) 401.
[20] N. Agmon and J.J. Hopfield, J. Chem. Phys. 79 (1983) 2042.
[21] N. Agmon and R. Kosloff, J. Phys. Chem. 91 (1987) 1988.
[22] V. Srajer, L. Reinisch and P.M. Champion, J. Am. Chem. Soc. 110 (1988) 6656.
[23] W. Bialek and R.F. Goldstein, Biophys. J. 48 (1985) 1027.
[24] D.L. Stein, Proc. Natl. Acad. Sci. USA 82 (1985) 3670.
[25] J.O. Alben, D. Beece, S.F. Bowne, W. Doster, L. Eisenstein, H. Frauenfelder, D. Good, D. McDonald, M.C. Marden, P.P. Moh, L. Reinisch, A.H. Reynolds, E. Shyamsunder and K.T. Yue, Proc. Natl. Acad. Sci. USA 79 (1982) 3744.
[26] J. Kuriyan, S. Wilz, M. Karplus and G.A. Petsko, J. Mol. Biol. 192 (1986) 133.
[27] D.P. Braunstein, Thesis, University of Illiois (1991).
[28] P. Ormos, D. Braunstein, H. Frauenfelder, M.K. Hong, S.-L. Lin, T.B. Sauke and R.D. Young, Proc. Natl. Acad. Sci. USA 85 (1988) 8492.
[29] J.N. Moore, P.A. Hansen and R.M. Hochstrasser, Proc. Natl. Acad. Sci. USA 85 (1988) 5062.
[30] P.A. Hansen, J.N. Moore and R.M. Hochstrasser, Chem. Phys. 131 (1989) 49.
[31] J. Hoinkis, R. Ahlrichs and H.-J. Böhm, Intern. J. Quantum Chem. 23 (1983) 821.
[32] J.L. Martin, A. Migus, C. Poyart, Y. Lecarpentier, R. Astier and A. Antonetti, Proc. Natl. Acad. Sci. USA 80 (1983) 173.
[33] J.W. Petrich, C. Poyart and J.L. Martin, Biochemistry 27 (1988) 4049.
[34] E.R. Henry, M. Levitt and W.A. Eaton, Proc. Natl. Acad. Sci. USA 82 (1985) 2034.
[35] J.W. Petrich, J.-C. Lambry, K. Kuczera, M. Karplus, C. Poyart, and J.-L. Martin, Biochemistry 30 (1991) 3975.
[36] P.A. Anfinrud, C. Han and R.M. Hochstrasser, Proc. Natl. Acad. Sci. USA 86 (1989) 8387.
[37] E. Antonini and M. Brunori, Hemoglobin and Myoglobin and Their Reactions with Ligands (North-Holland, Amsterdam, 1971).
[38] B.I. Greene, R.M. Hochstrasser, R.B. Weisman and W.A. Eaton, Proc. Natl. Acad. Sci. USA 75 (1978) 5255.
[39] T. Takano, J. Mol. Biol. 110 (1977) 569.
[40] J.C. Norvell, A.C. Nunes and B.P. Schoenborn, Science 190 (1975) 568.
[41] M. Ikeda-Saito, T. Iizuka, H. Yama, F.J. Kayne and T. Yonetani, J. Biol. Chem. 252 (1977) 4882.
[42] F.G. Fiamingo and J.O. Alben, Biochemistry 24 (1985) 7964.
[43] S. Phillips and B.P. Schoenborn, Nature 292 (1981) 81.
[44] B.R. Brooks, R.E. Bruccoleri, B.D. Olafson, D.J. States, S. Swaminathan and M. Karplus, J. Comput. Chem. 4 (1983) 187.
[45] C.L. Brooks III, B.M. Pettitt and M. Karplus, J. Chem. Phys. 83 (1985) 5897.
[46] B.R. Brooks and M. Karplus, Proc. Natl. Acad. Sci. USA 82 (1985) 4995.
[47] R.J. Loncharich and B.R. Brooks, Proteins 6 (1989) 32.

[48] J.B. Matthew and F.R.N. Gurd, Meth. Enzymol. 130 (1986) 413.
[49] B.J. Berne and G.D. Harp, Advan. Chem. Phys. 17 (1970) 63.
[50] P.F. Fracassi and R.G. Della Valle, Chem. Phys. Letters 104 (1984) 435.
[51] P.F. Fracassi, R. Righini, R.G. Della Valle and M.L. Klein, Chem. Phys. 96 (1985) 361.
[52] J.N. Huffaker, J. Chem. Phys. 64 (1975) 3175; 64 (1976) 4564.
[53] P.H. Berens and K.R. Wilson, J. Chem. Phys. 74 (1981) 4872.
[54] B.H. Mahan, College Chemistry (Addison-Wesley, Reading, MA, 1966).
[55] D. Oxtoby, Advan. Chem. Phys. 40 (1979) 1.
[56] A.T. Brünger, C.L. Brooks III and M. Karplus, Proc. Natl. Acad. Sci. USA 82 (1985) 8458.
[57] C.L. Brooks III and M. Karplus, J. Chem. Phys. 79 (1983) 6312.
[58] C.L. Brooks III and M. Karplus, J. Mol. Biol. 205 (1989) 159.
[59] W.F. van Gunsteren and H.J.C. Berendsen, Mol. Phys. 34 (1977) 1311.
[60] W.L. Jorgensen, J. Chandrasekhar, J.D. Madura, R.W. Impey and M.L. Klein, J. Chem. Phys. 79 (1983) 926.
[61] C.L. Brooks III, A.T. Brünger and M. Karplus, Biopolymers 24 (1985) 843.
[62] W.H. Press, B.P. Flannery, S.A. Teukolsky and W.T. Vetterling, Numerical Recipes: The Art of Scientific Computing (Cambridge Univ. Press, Cambridge, 1986).
[63] R.E. Levine and R.B. Bernstein, Molecular Reaction Dynamics and Chemical Reactivity (Oxford Univ. Press, Oxford, 1987) p. 312.
[64] J. Metiu, D.W. Oxtoby and K.F. Freed, Phys. Rev. A 15 (1977) 361.
[65] D.J. Deistler, Chem. Phys. Letters 39 (1976) 39; Advan. Chem. Phys. 42 (1980) 305.
[66] D.J. Nesbitt and J.T. Hynes, J. Chem. Phys. 77 (1982) 2130.
[67] S.A. Adelman, Advan. Chem. Phys. 53 (1983) 61.
[68] R.G. Gordon, Advan. Magn. Reson. 3 (1968) 1.
[69] R.G. Gordon, J. Chem. Phys. 44 (1966) 1830.
[70] B.J. Berne and R. Pecora, Dynamic Light Scattering (Wiley-Interscience, New York, NY, 1976).
[71] G.E. Ewing, J. Chem. Phys. 37 (1962) 2250.
[72] G.J. Jiang, W.B. Person and K.G. Brown, J. Chem. Phys. 62 (1975) 1201.
[73] H. Dubost and L. Abouaf-Marguin, Chem. Phys. Letters 17 (1972) 269.
[74] M.F. Herman and B.J. Berne, J. Chem. Phys. 78 (1983) 4103.
[75] K.F. Schweizer and D. Chandler, J. Chem. Phys. 76 (1982) 2296.
[76] (a) W.J. Hehre, L. Radom, P.V.R. Schleyer and J.A. Pople, Ab Initio Molecular Orbital Theory (Wiley, New York, 1986).
(b) J.D. Augsburger, C.E. Dykstra and E. Oldfield, J. Am. Chem. Soc. 113 (1991) 2447.
[77] L. Pauling, The Nature of the Chemical Bond (Cornell Univ. Press. Ithaca, NY, 1960).
[78] J.E. Huheey, Inorganic Chemistry (Harper & Row, New York, 1978).
[79] J. Gebicki and A. Krantz, J. Am. Chem. Soc. 106 (1984) 8093; 106 (1984) 8097.
[80] D. Braunstein, B.R. Cowen, K.D. Egeberg, H. Frauenfelder, J. Mourant, P. Ormos, S.G. Sligar, B.A. Springer and R.D. Young, Biophys. J. 55 (1989) 565a.
[81] D. Braunstein, A. Ansari, J. Berendzen, B.R. Cowen, K.D. Egeberg, H. Frauenfelder, M.K. Hong, P. Ormos, T.B. Sauke, R. Scholl, A. Schulte, S.G. Sliger, B.A. Springer, P.J. Steinbach and R.D. Young, Proc. Natl. Acad. Sci. USA 85 (1988) 8497.
[82] P.E. Stogryn and A.P. Stogryn, Mol. Phys. 11 (1966) 371.
[83] C. Chackerian Jr., J. Chem. Phys. 65 (176) 4228.
[84] W. Reiher, Ph.D. Thesis, Harvard University (1982).
[85] W.L. Jorgensen, J. Am. Chem. Soc. 90 (1986) 1276.
[86] D.L. Beveridge and F.M. DiCapua, Annu. Rev. Biophys. Biophys. Chem. 18 (1989) 431.
[87] E. Wilhelm, R. Battino and R.J. Wilcock, Chem. Rev. 77 (1977) 219.
[88] J.O. Hirschfelder, C.F. Curtiss and R.B. Bird, Molecular Theory of Gases and Liquids (Wiley, New York, 1954).
[89] L. Rothberg, T.M. Jedju and R.H. Austin, Biophys. J. 57 (1990) 369.